

Order a improved renormalization constants

Tanmoy Bhattacharya,^{1,*} Rajan Gupta,^{1,†} Weonjong Lee,^{1,‡} and Stephen Sharpe^{2,§}

¹*Theoretical Division, Los Alamos National Lab,
Los Alamos, New Mexico 87545, USA*

²*Physics Department, University of Washington, Seattle, Washington 98195, USA*

Abstract

We present non-perturbative results for the constants needed for on-shell $O(a)$ improvement of bilinear operators composed of Wilson fermions. We work at $\beta = 6.0$ and 6.2 in the quenched approximation. The calculation is done by imposing axial and vector Ward identities on correlators similar to those used in standard hadron mass calculations. A crucial feature of the calculation is the use of non-degenerate quarks. We also obtain results for the constants needed for off-shell $O(a)$ improvement of bilinears, and for the scale and scheme independent renormalization constants, Z_A , Z_V and Z_S/Z_P . Several of the constants are determined using a variety of different Ward identities, and we compare their relative efficacies. In this way, we find a method for calculating c_V that gives smaller errors than that used previously. Where possible, we compare our results with those of the ALPHA collaboration (who use the Schrödinger functional) and with 1-loop tadpole-improved perturbation theory.

*Electronic address: tanmoy@lanl.gov; URL: <http://t8web.lanl.gov/t8/people/tanmoy/>

†Electronic address: rajan@lanl.gov; URL: <http://t8web.lanl.gov/t8/people/rajan/>

‡Electronic address: wlee@lanl.gov; URL: <http://t8web.lanl.gov/t8/people/wlee/>

§Electronic address: sharpe@phys.washington.edu

I. INTRODUCTION

Symanzik's improvement program is a systematic method for reducing discretization errors in lattice simulations [1, 2]. One must improve both the action and external operators by the addition of appropriate higher dimension localized operators. Complete removal of discretization errors at a given order in the lattice spacing, a , requires a non-perturbative determination of the coefficients (the “improvement constants”) of the higher dimension operators. A key ingredient in the practical implementation of the improvement program is the development of methods for such non-perturbative determinations.

The ALPHA collaboration has exploited the connection between $O(a)$ discretization errors and chiral symmetry to develop non-perturbative methods for the calculation of some of the $O(a)$ improvement constants (those for the action and some of the local fermion bilinear operators) [3, 4, 5, 6]. Their approach is based on the imposition of axial and vector Ward identities. It also determines the renormalization-scale independent normalization constants Z_A^0 , Z_V and Z_S^0/Z_P^0 , as originally observed in Ref. 7. This non-perturbative determination of improvement and normalization constants is of considerable practical importance, as uncertainties in these constants can be a significant source of error in lattice calculations of matrix elements.

In Ref. 8 we showed how to extend the method of the ALPHA collaboration to determine all the $O(a)$ improvement constants for bilinears.¹ The extension involves the enforcement of Ward identities for massive, non-degenerate quarks, rather than in the chiral limit, and is a generalization of the method of Ref. 11. Results of a pilot simulation at $\beta = 6$ (quenched) suggested that the method was practical. This simulation had the drawback, however, that it was done using tadpole-improved, rather than non-perturbatively improved, Wilson fermions. Thus a clean separation of sources of error was not possible.

In this paper we present results of a more extensive investigation of the method. We use the non-perturbatively improved action, taking the non-perturbative value for the Sheikholeslami-Wohlert (or “clover”) coefficient c_{SW} [12] from the work of the ALPHA collaboration [3]. Thus the errors after improvement should be of $O(a^2)$. We study the scaling behavior of improvement and normalization constants by carrying out the calculation at two values of the lattice spacing, $\beta = 6$ and 6.2 (quenched). We also extend previous work by determining the improvement coefficients for the operators which vanish by the equations of motion (“equation-of-motion operators”). These contribute only to off-shell matrix elements, and thus are not of direct physical relevance, but they do contribute to the Ward Identities at non-zero quark masses.

As already noted, several of the improvement and renormalization constants that we determine have been previously obtained by the ALPHA collaboration. An important difference in the implementation of the improvement conditions is that the ALPHA collaboration uses Schrödinger functional boundary conditions with sources on the boundary, while we use periodic boundary conditions with standard sources for quark propagators designed to improve overlap of local operators with hadronic ground states. This means that the results for improvement constants will differ at $O(a)$ and the normalization constants will differ at $O(a^2)$. One of the aims of our study is to compare results from the two approaches, since this gives an indication of the importance of the neglected higher order terms. We can also

¹ Other approaches that allow one to determine, in principle, all the improvement and normalization constants have been suggested in Refs. 9, 10.

get some idea of the relative effectiveness of the two approaches.

The organization of this paper is as follows. In the following section we briefly recapitulate the theoretical background to our method, and give a general description of our implementation. Sec. III contains a summary of our simulation parameters. In Sec. IV, we present our final results, and discuss their implications. We reserve a detailed discussion of the calculation of the individual improvement coefficients for Secs. V–XII. We close with some conclusions in Sec. XIII. Three appendices collect the tadpole-improved perturbative results which we use for comparison with our non-perturbative estimates, the tree-level definitions of the improvement constants, and a discussion of exceptional configurations.

II. WARD IDENTITIES: THEORETICAL BACKGROUND

On-shell improvement of bilinear operators at $O(a)$ requires both the addition of extra operators,

$$\begin{aligned} (A_I)_\mu &\equiv A_\mu + ac_A \partial_\mu P \\ (V_I)_\mu &\equiv V_\mu + ac_V \partial_\nu T_{\mu\nu} \\ (T_I)_{\mu\nu} &\equiv T_{\mu\nu} + ac_T (\partial_\mu V_\nu - \partial_\nu V_\mu) \\ P_I &\equiv P \\ S_I &\equiv S, \end{aligned} \tag{1}$$

and the introduction of the following mass dependence

$$\mathcal{O}_R^{(ij)} \equiv Z_{\mathcal{O}}^0 (1 + b_{\mathcal{O}} a m_{ij}) \mathcal{O}_I^{(ij)}, \tag{2}$$

$$\equiv Z_{\mathcal{O}}^0 (1 + \tilde{b}_{\mathcal{O}} a \tilde{m}_{ij}) \mathcal{O}_I^{(ij)}. \tag{3}$$

Here (ij) (with $i \neq j$) specifies the flavor, and $\mathcal{O} = A, V, P, S, T$. The $Z_{\mathcal{O}}^0$ are renormalization constants in the chiral limit, $m_{ij} \equiv (m_i + m_j)/2$ is the average bare quark mass,² and \tilde{m}_{ij} is the quark mass defined in Eq. (15) using the axial Ward identity (AWI). There are yet other improvement constants needed in order to extend the analyses to flavor-neutral bilinears ($i = j$) and to full QCD. These extensions are discussed in Ref. 13, but are not relevant here. Note that, except in Appendix B, we have set the Wilson parameter r equal to unity.

When improving the theory to $O(a)$, one still has freedom in defining the $c_{\mathcal{O}}$ and the $b_{\mathcal{O}}$. For example, in general, they can depend on the correlators used to define them and on the quark mass. We shall consistently use the value in the chiral limit as it is the simplest choice and is also the one made in previous work by other collaborations. The correlators used to define them are discussed in subsequent sections.

To avoid confusion, we stress that the coefficients $\tilde{b}_{\mathcal{O}}$ differ from the $b_{\mathcal{O}}$ used by earlier authors. In particular, at the level of $O(a)$ improvement, one has

$$\tilde{b}_{\mathcal{O}} = (Z_A^0 Z_S^0 / Z_P^0) b_{\mathcal{O}}. \tag{4}$$

² The bare quark masses are $am_i = 1/2\kappa_i - 1/2\kappa_c$, κ being the hopping parameter in the Sheikholeslami–Wohlert action and κ_c its value in the chiral limit.

The analogous relation between m and \tilde{m} is given in Eq. (27).

Improvement can be achieved by imposing the generic axial Ward identity

$$\langle \delta S^{(12)} \mathcal{O}_{R,off}^{(23)}(y) J^{(31)}(0) \rangle = \langle \delta \mathcal{O}_{R,off}^{(13)}(y) J^{(31)}(0) \rangle \quad (5)$$

for enough choices of J , \mathcal{O} , and y to determine all the relevant improvement and scale independent normalization constants. This should then guarantee that the identity holds up to corrections of $O(a^2)$ for other choices of J and y . Here $\delta\mathcal{O}$ is the bilinear which results from the axial variation of \mathcal{O} in the continuum ($A_\mu \leftrightarrow V_\mu$, $S \leftrightarrow P$, and $T_{\mu\nu} \rightarrow \epsilon_{\mu\nu\rho\sigma} T_{\rho\sigma}$), and the variation of the action under an axial rotation is

$$\delta S^{(12)} = Z_A^{(12)} \int_V d^4x \left[(2\tilde{m}_{12})(P_{I,off})^{(12)} - \partial_\mu (A_{I,off})_\mu^{(12)} \right]. \quad (6)$$

The point y lies within the domain, V , of the chiral rotation, while the source J is located outside V .

To implement Eq. (5) away from the chiral limit, it is not sufficient to use the on-shell improved bilinears, \mathcal{O}_R , defined in Eqs. (2,3). One must also include dimension 4 operators which vanish by the equations of motion, and this has been anticipated in the use of the subscript *off*. As noted in Ref. 9, there is one such operator with the appropriate symmetries for each bilinear:

$$\mathcal{O}_{R,off}^{(ij)} = Z_{\mathcal{O}}^{(ij)} \mathcal{O}_{I,off}^{(ij)}, \quad (7)$$

$$\mathcal{O}_{I,off}^{(ij)} = \mathcal{O}_I^{(ij)} - a \frac{1}{4} c'_{\mathcal{O}} E_{\mathcal{O}}^{(ij)}, \quad (8)$$

$$E_{\mathcal{O}}^{(ij)} = \overline{\psi}^{(i)} \Gamma \vec{\mathcal{W}} \psi^{(j)} - \overline{\psi}^{(i)} \vec{\mathcal{W}} \Gamma \psi^{(j)}. \quad (9)$$

In the equation-of-motion operators $E_{\mathcal{O}}$, Γ is the Dirac matrix defining \mathcal{O} , and $\vec{\mathcal{W}}\psi_j = (\vec{\mathcal{D}} + m_j)\psi_j + O(a^2)$ is defined to be the full $O(a)$ improved Dirac operator for quark flavor j (see Appendix B). This ensures that $E_{\mathcal{O}}$ gives rise only to contact terms, and thus cannot change the overall normalization $Z_{\mathcal{O}}$. The factors multiplying $E_{\mathcal{O}}$ are chosen such that, at tree level, $c'_{\mathcal{O}} = 1$ for all Dirac structures as shown explicitly in Appendix B.

For practical applications, it is useful to express the Ward identity in terms of on-shell improved operators. The equation-of-motion operators contribute only when the operators P (contained in δS) and \mathcal{O} , in the l.h.s. of Eq. (5), coincide. The γ_5 in $P_{I,off}$ changes $\mathcal{O}_{I,off}$ to $\delta\mathcal{O}_{I,off}$, and so, up to $O(a^2)$ corrections, these contact terms are proportional to the r.h.s. of Eq. (5). After rearrangement, one finds

$$\frac{\langle \int_V d^4x \delta S_I \mathcal{O}_I^{(23)}(y_4, \vec{y}) J^{(31)}(0) \rangle}{\langle \delta \mathcal{O}_I^{(13)}(y_4, \vec{y}) J^{(31)}(0) \rangle} = \frac{Z_{\delta\mathcal{O}}^{(13)}}{Z_A^{(12)} Z_{\mathcal{O}}^{(23)}} + a \frac{c'_P + c'_{\mathcal{O}}}{2} \tilde{m}_{12} + O(a^2) \quad (10)$$

where

$$\delta S_I(x) \equiv 2\tilde{m}_{12} P_I^{(12)}(x) - \partial_\mu (A_I)_\mu^{(12)}(x). \quad (11)$$

This is the form of the AWI which we enforce (*i.e.* for some choice of J we fit to a range in y , neglecting $O(a^2)$ contributions) in order to determine the improvement constants. Note that the mass multiplying the c' coefficients is \tilde{m} and not m . Also, for brevity, mention of the $O(a^2)$ terms in all equations is henceforth omitted.

To highlight the dependence on quark masses, the r.h.s. of Eq. (10) can be written as

$$RHS = \frac{Z_{\delta\mathcal{O}}^0}{Z_A^0 Z_{\mathcal{O}}^0} \left[1 + a\tilde{b}_{\delta\mathcal{O}}\tilde{m}_{13} - ab_A\tilde{m}_{12} - ab_{\mathcal{O}}\tilde{m}_{23} \right] + a\frac{c'_P + c'_{\mathcal{O}}}{2}\tilde{m}_{12}, \quad (12)$$

and, in the special case $\tilde{m}_1 = \tilde{m}_2$ relevant to our numerical study, as

$$\begin{aligned} RHS = & \frac{Z_{\delta\mathcal{O}}^0}{Z_A^0 Z_{\mathcal{O}}^0} \left[1 + (\tilde{b}_{\delta\mathcal{O}} - \tilde{b}_{\mathcal{O}}) \frac{a\tilde{m}_3}{2} \right] \\ & + \left[\frac{Z_{\delta\mathcal{O}}^0}{Z_A^0 Z_{\mathcal{O}}^0} \left(\frac{(\tilde{b}_{\delta\mathcal{O}} - \tilde{b}_{\mathcal{O}})}{2} - \tilde{b}_A \right) + \frac{c'_P + c'_{\mathcal{O}}}{2} \right] a\tilde{m}_1. \end{aligned} \quad (13)$$

Here we have defined $\tilde{m}_i = \tilde{m}_{ij}|_{m_j=m_i}$, *i.e.* \tilde{m}_i is the AWI mass with two degenerate quarks of bare mass m_i .

In our lattice simulations we calculate the l.h.s. of Eq. (10) as a function of $\tilde{m}_1 = \tilde{m}_2$ and \tilde{m}_3 , and extract the various constants using the following procedure. In the first step of the analyses we remove the contribution of the equation-of-motion operators by extrapolating the l.h.s to $\tilde{m}_1 = 0$, for fixed \tilde{m}_3 . The ratio $X_{\mathcal{O}} \equiv Z_{\delta\mathcal{O}}^0/Z_A^0 Z_{\mathcal{O}}^0$ is then given by the intercept of a linear fit in $\tilde{m}_3/2$, while the slope gives $X_{\mathcal{O}}(\tilde{b}_{\delta\mathcal{O}} - \tilde{b}_{\mathcal{O}})$. By choosing operators with different Dirac structures we are able to extract all the on-shell improvement constants, as well as Z_A , Z_V and Z_P/Z_S . The only exception is b_T , which as discussed in Ref. 8, requires keeping $\tilde{m}_1 \neq \tilde{m}_2$.

This analysis ignores $O(a^2)$ terms. Since these can give rise to a quadratic dependence on quark mass, it is important to check that linear fits are adequate. In cases where the statistical quality of the data is good we compare linear and quadratic fits. Another check on the importance of $O(a^2)$ terms is to repeat the fits using the mass m_3 instead of \tilde{m}_3 . In this case the ratio of slope to intercept gives $b_{\delta\mathcal{O}} - b_{\mathcal{O}}$, which we can then compare to the results for $\tilde{b}_{\delta\mathcal{O}} - \tilde{b}_{\mathcal{O}}$ using Eq. (4). This comparison is non-trivial since the $O(a^2)$ effects are different in the two cases. We stress, however, that, unless otherwise stated, the results presented below are from fits with respect to \tilde{m}_3 .

We note that, up to this point in the analysis, we do not need to introduce the off-shell improved operators. When we send $\tilde{m}_1 = \tilde{m}_2 \rightarrow 0$ we are removing the contact term between P and \mathcal{O} 8, and so on-shell improved operators suffice.

This is no longer true, however, in the second step of our analysis. Here we keep $\tilde{m}_1 = \tilde{m}_2$ non-zero, so the contact term remains. We determine the linear combination $c'_P + c'_{\mathcal{O}}$ from the slope, $s_{\mathcal{O}}$, of a linear fit of the l.h.s. of Eq. (10) with respect to $a\tilde{m}_1$ at fixed $a\tilde{m}_3$. In this way, for each $a\tilde{m}_3$, we obtain the estimate

$$c'_P + c'_{\mathcal{O}} = 2s_{\mathcal{O}} - X_{\mathcal{O}}(\tilde{b}_{\delta\mathcal{O}} - \tilde{b}_{\mathcal{O}} - 2\tilde{b}_A). \quad (14)$$

By choosing $\mathcal{O} = S, P, A, V, T$ we can determine all five $c'_{\mathcal{O}}$. Details of this part of the calculation are presented in Sec. XII.

III. SIMULATION PARAMETERS

The parameters used in the three sets of simulations are given in Tab. I. The table also gives the labels used to refer to the different simulations in the following. For the lattice

Label	β	c_{SW}	a^{-1} (GeV)	Volume	L (fm)	Confs.	x_4
60TI	6.0	1.4755	2.12	$16^3 \times 48$	1.5	83	$4 - 18$
60NPf	6.0	1.769	2.12	$16^3 \times 48$	1.5	125	$4 - 18$
60NPb						112	$27 - 44$
62NP	6.2	1.614	2.91	$24^3 \times 64$	1.65	70	$6 - 25$
						70	$39 - 58$

TABLE I: Simulation parameters, statistics, and the time interval in x_4 defining the volume V over which the chiral rotation is performed in the AWI. The source J is placed at $t = 0$.

scale a we have taken the value determined in Ref. 14 using r_0 , as it does not rely on the choice of the fermion action for a given β . In this study what we mostly need is the change in scale, $a(\beta = 6.2)/a(\beta = 6.0) \approx 0.73$, which is much less sensitive to the physical quantity used to set a .

In Tab. II we give the values of the hopping parameter κ we use, along with the corresponding results for $a\tilde{m}$ and aM_π . We also quote three estimates of κ_c , obtained using quadratic fits, corresponding to (1) the zero of \tilde{m} with mass independent c_A (see Sec. V), (2) the zero of \tilde{m} with chirally extrapolated c_A , and (3) the zero of M_π^2 . These are labeled $\kappa_c^{(1)}$, $\kappa_c^{(2)}$, and $\kappa_c^{(3)}$ respectively. In this paper we use $\kappa_c^{(1)}$ henceforth and drop the superscript.

For each set of simulation parameters the quark propagators are calculated using Wuppertal smearing [15]. The hopping parameter in the 3-dimensional Klein-Gordon equation used to generate the gauge-invariant smearing is set to 0.181, which gives mean squared smearing radii of $(ra)^2 = 2.9$ and 3.9 for $\beta = 6.0$ and 6.2 respectively.

For the **60NP** data set we have investigated the dependence of our results on the time extent of the region of chiral rotation. As shown in Tab. I, one region (forward of the source) is 15 timeslices long, while the other (backward of the source) is 18 slices long. Since we find no significant dependence on the length of the time interval, we average the two sets of results (assuming statistical independence). In the **62NP** calculation, we also use two rotation regions, this time placed symmetrically about the source, in order to improve the signal.

In the **60NP** data set we find two exceptional configurations. Some details of the behavior of the pion correlator on these configurations are discussed in Appendix C. The effect is most severe at the lightest quark mass, κ_7 . We do not discard these configurations, but we do neglect all data with the lightest two quark masses, *i.e.*, the κ_6 and κ_7 points are not used in the final analyses of **60NPf** and **60NPb** data. In the analysis of the **60TI** data we exclude κ_1 and κ_7 since the former is too heavy and the latter may have contamination from exceptional configurations.

IV. RESULTS

We begin with some general comments concerning our analysis. First, all our quoted results are obtained using correlation functions at zero spatial momentum. We have numerical data for non-zero momentum correlators, which lead to consistent results but with larger errors. Second, we use only the diagonal part of the covariance matrix when fitting the time dependence of correlators, or of ratios of correlators. Fits using the full covariance

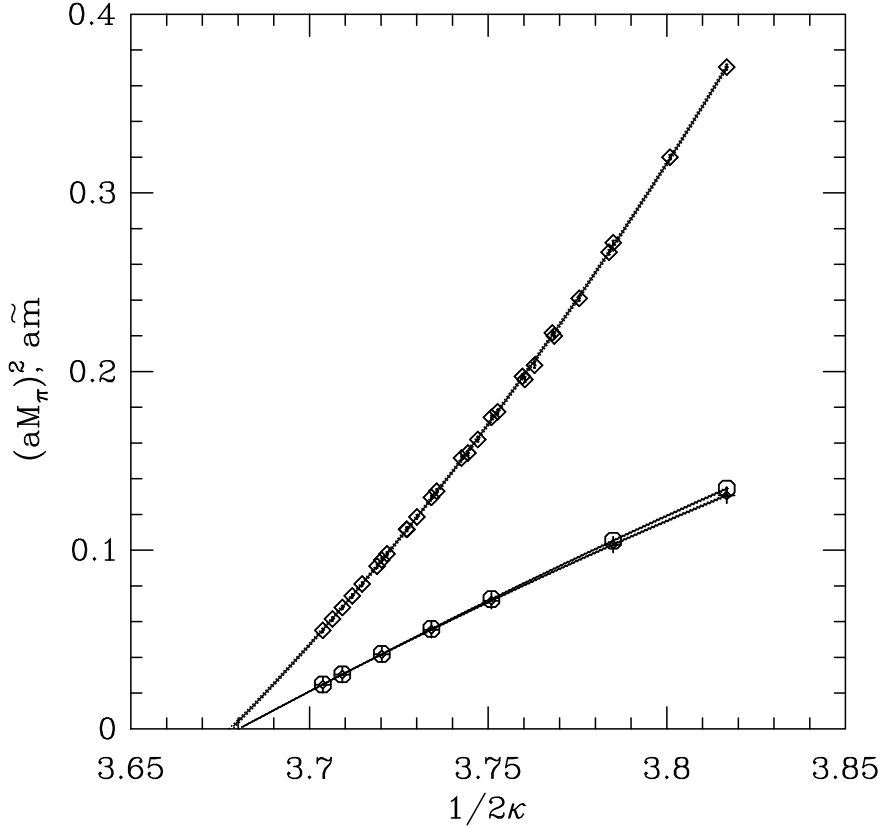


FIG. 1: Estimates of κ_c by extrapolating **62NP** data for \tilde{m} and M_π^2 . We show quadratic fits to \tilde{m} for the two cases discussed in text (octagons label points with mass-dependent c_A and pluses label points with chirally extrapolated c_A), and a quadratic fit to M_π^2 (diamonds).

matrix (which incorporates the correlations between timeslices) were not, in general, stable. Where we could perform such fits, we found results within 1σ of those presented. Finally, fits to the quark mass dependence are also done ignoring correlations between the points at different masses, since our statistics are insufficient to include them. Because of the latter two comments, we can make no quantitative statement about goodness of fit. Nevertheless, assuming that the fits are good, the errors in the fit parameters, which are obtained using the Jackknife procedure, should be reliable.

We begin with our results for κ_c , which is needed to define the vector Ward identity (VWI) quark mass m . To determine κ_c , we make a quadratic fit of the AWI mass, \tilde{m} , and M_π^2 versus the tree-level quark mass parameter $1/2\kappa$. Fits to \tilde{m} include only degenerate quark combinations as it simplifies Eq. (27). Fits to M_π^2 include both degenerate and non-degenerate combinations as they do not show any noticeable dependence on the mass difference. For the non-degenerate cases we define $2/\kappa_{ij} = 1/\kappa_i + 1/\kappa_j$. An example of the resulting fits is shown in Fig. 1. The estimate of κ_c from \tilde{m} should be the same whether we use the mass-dependent value for c_A or the chirally extrapolated value in Eq. (15) (see Sec. V). As evident from Fig. 1, the quality of both these fits is very similar and the two values are consistent.

Our results for $1/\kappa_c$ from quadratic fits to M_π^2 are significantly smaller than those from fits to \tilde{m} . To highlight this discrepancy we present, in Tab. II, the values of aM_π at the

Label	60TI			60NP			62NP		
	κ	$a\tilde{m}$	aM_π	κ	$a\tilde{m}$	aM_π	κ	$a\tilde{m}$	aM_π
κ_1	0.11900	0.443(8)	1.530(1)	0.1300	0.144(1)	0.711(2)	0.1310	0.1345(6)	0.609(1)
κ_2	0.13524	0.105(1)	0.571(2)	0.1310	0.118(1)	0.630(2)	0.1321	0.1054(4)	0.522(1)
κ_3	0.13606	0.084(1)	0.504(2)	0.1320	0.092(1)	0.544(2)	0.1333	0.0727(3)	0.418(1)
κ_4	0.13688	0.063(1)	0.431(2)	0.1326	0.075(1)	0.488(2)	0.1339	0.0560(2)	0.360(2)
κ_5	0.13770	0.042(1)	0.348(3)	0.1333	0.056(1)	0.416(2)	0.1344	0.0419(2)	0.307(2)
κ_6	0.13851	0.020(1)	0.244(4)	0.1342	0.032(1)	0.308(3)	0.1348	0.0306(2)	0.261(2)
κ_7	0.13878	0.013(1)	0.195(8)	0.1345	0.025(4)	0.262(12)	0.1350	0.0248(1)	0.235(2)
$\kappa_c^{(1)}$	0.13926(2)	0	0.082(15)	0.13532(3)	0	0.083(20)	0.135861(5)	0	0.066(10)
$\kappa_c^{(2)}$	0.13925(2)	0	0.086(15)	0.13530(1)	0	0.106(16)	0.135862(4)	0	0.073(09)
$\kappa_c^{(3)}$	0.13934(4)			0.13541(3)			0.13594(2)		

TABLE II: Values of the hopping parameter used in the various simulations, and the corresponding pseudoscalar mass aM_π and quark mass $a\tilde{m}$ defined using the mass-dependent c_A (see Sec. V). The three estimates of κ_c , obtained using quadratic fits, correspond to (1) the zero of \tilde{m} with mass dependent c_A , (2) the zero of \tilde{m} with chirally extrapolated c_A , and (3) the zero of M_π^2 . We quote the extrapolated value of aM_π for cases (1) and (2).

κ_c determined from fits to \tilde{m} . Such a discrepancy has been observed previously (see, *e.g.*, Ref. 16), and can be attributed to a combination of quenched chiral logarithms (the effect of which is to cause M_π^2 to curve downward at small quark masses [17, 18]) and chiral symmetry breaking by the action (which allows $aM_\pi(\tilde{m} = 0) \propto a^{3/2}$ and a^2 effect, respectively, for tadpole-improved and non-perturbatively improved actions). These contributions can, in principle, be distinguished by the behavior of the intercept $aM_\pi(\tilde{m} = 0)$. Quenched chiral logarithms are a continuum effect, implying that the intercept should be the same for **60 TI** and **60NP** simulations, and that it should scale roughly proportional to a . By contrast, explicit chiral symmetry breaking implies a reduction in the intercept when going from **60TI** to **60NP** data sets, and an a^2 scaling in **NP** simulations. In our analyses this latter effect is expected to be small since \tilde{m} is determined by a fit over a large range of time slices where the pion dominates. If these fits had extended to $t = \infty$, then \tilde{m} and M_π would necessarily vanish at the same κ . Our results are consistent with the dependence expected from quenched chiral logarithms. The large residual M_π , therefore, points to the need to include the effect of quenched chiral logarithms in the extrapolation.

From the fit \tilde{m} versus $1/2\kappa$ we also obtain the combination $(b_P - b_A + b_m)$ using Eq. (27). This is discussed in Sec. XI.

In Tabs. III, IV, V, and VI, we collect our results from the various Ward identities, except for estimates of c_V which are given in Tab. VII. Each identity allows us to extract one or more combinations of on-shell improvement and normalization constants. The details of each of these extractions are discussed in subsequent sections. From these results, we construct our best estimates for the individual constants, and these are collected in Tab. VIII. We quote both a statistical error (obtained by single elimination jackknife, in which we repeat the entire analysis on each jackknife sample), and an estimate of the uncertainty in the constants due to $O(a^2)$ errors. The latter is obtained by comparing results using values of c_A deduced using 2-point and 3-point discretizations of derivatives, as discussed in the

	reference	2-point	3-point
c_A	Eq.(15)	-0.022(06)	-0.023(09)
Z_V^0	Eq.(17)	+0.747(01)	+0.747(01)
\tilde{b}_V	Eq.(17)	+1.436(27)	+1.455(28)
Z_V^0	Eq.(17)	+0.747(01)	+0.747(01)
b_V	Eq.(17)	+1.534(24)	+1.535(24)
$Z_P^0/Z_A^0 Z_S^0$	Eq.(18,19)	+1.068(13)	+1.056(14)
Z_V^0	Eq.(22)	+0.755(06)	+0.759(06)
$\tilde{b}_A - \tilde{b}_V$	Eq.(22)	-0.513(91)	-0.477(95)
Z_V^0	Eq.(22)	+0.756(06)	+0.760(06)
$b_A - b_V$	Eq.(22)	-0.488(85)	-0.452(89)
$Z_V^0/(Z_A^0)^2$	Eq.(25)	+1.207(15)	+1.196(16)
$\tilde{b}_A - \tilde{b}_V$	Eq.(25)	-0.668(216)	-0.566(222)
Z_A^0	Eq.(20,25)	+0.791(07)	+0.787(07)
$Z_P^0/Z_A^0 Z_S^0$	Eq.(26)	+1.029(10)	+1.026(13)
$Z_P^0/Z_A^0 Z_S^0$	Eq.(27)	+1.066(14)	+1.054(15)
$\tilde{b}_P - \tilde{b}_S$	Eq.(26)	-0.070(88)	-0.055(89)
c_T	Eq.(30)	+0.087(15)	+0.099(18)
$\tilde{b}_A - \tilde{b}_P + \tilde{b}_S/2 [c_A(m)]$	Eq.(27)	+0.739(66)	+0.703(75)
$\tilde{b}_A - \tilde{b}_P + \tilde{b}_S/2 [c_A(0)]$	Eq.(27)	+0.879(64)	+0.021(46)
$\tilde{b}_P - \tilde{b}_A$	Eq.(31)	-0.126(58)	-0.125(81)
$\tilde{b}_S - \tilde{b}_V - 2(\tilde{b}_P - \tilde{b}_A)$	Eq.(32)	-0.588(274)	-0.266(380)

TABLE III: Results for the **60TI** data set.

following section. Another estimate of $O(a^2)$ errors is obtained by comparing our results to the previous estimates of the ALPHA collaboration [4, 5, 6] which we also include in Tab. VIII along with the one-loop perturbative results discussed in Appendix A. We quote both \tilde{b}_V, \tilde{b}_A and b_V, b_A to simplify comparison with previous results.

We collect separately, in Tab. IX, our results for the improvement constants c'_X , the coefficients of the equation-of-motion operators. These are discussed in Sec. XII.

The assiduous reader will notice that our results for the **60TI** data differ slightly from those presented in Ref. 8. This is for two reasons. First, we use a new method for determining c_V . This leads to a much more precise result, and affects several other analyses which are dependent on c_V . Second, we have made several minor improvements in our analysis, *e.g.* using quadratic instead of linear fits versus quark mass where appropriate. The set of configurations has not changed.

We now discuss the salient features of our final results from Tab. VIII. Perhaps the most important issue is the comparison with the results by the ALPHA collaboration. Because we use different improvement conditions, the results for the Z_X^0 can differ by $\sim a^2 \Lambda_{QCD}^2$, while those for the c_X and b_X can differ by $\sim a \Lambda_{QCD}$. Numerically these are about 0.02 and 0.15, respectively, at $\beta = 6.0$, and 0.01 and 0.1, respectively, at $\beta = 6.2$. There are some quantities, however, where these differences can be enhanced. For example, in correlators

	reference	2-point	3-point
c_A	Eq.(15)	-0.037(04)	-0.045(07)
Z_V^0	Eq.(17)	+0.770(01)	+0.769(01)
\tilde{b}_V	Eq.(17)	+1.429(20)	+1.466(24)
Z_V^0	Eq.(17)	+0.769(01)	+0.768(01)
b_V	Eq.(17)	+1.524(14)	+1.525(14)
$Z_P^0/Z_A^0 Z_S^0$	Eq.(18,19)	+1.067(09)	+1.041(13)
Z_V^0	Eq.(22)	+0.773(04)	+0.775(04)
$\tilde{b}_A - \tilde{b}_V$	Eq.(22)	-0.231(47)	-0.179(57)
Z_V^0	Eq.(22)	+0.774(03)	+0.776(04)
$b_A - b_V$	Eq.(22)	-0.216(43)	-0.165(53)
$Z_V^0/(Z_A^0)^2$	Eq.(25)	+1.197(09)	+1.185(10)
$\tilde{b}_A - \tilde{b}_V$	Eq.(25)	-0.193(91)	-0.180(107)
Z_A^0	Eq.(20,25)	+0.808(03)	+0.800(03)
$Z_P^0/Z_A^0 Z_S^0$	Eq.(26)	+1.048(09)	+1.035(11)
$Z_P^0/Z_A^0 Z_S^0$	Eq.(27)	+1.049(08)	+1.026(11)
$\tilde{b}_P - \tilde{b}_S$	Eq.(26)	-0.013(55)	+0.019(57)
c_T	Eq.(30)	+0.063(07)	+0.092(11)
$\tilde{b}_A - \tilde{b}_P + \tilde{b}_S/2 [c_A(m)]$	Eq.(27)	+0.609(31)	+0.570(53)
$\tilde{b}_A - \tilde{b}_P + \tilde{b}_S/2 [c_A(0)]$	Eq.(27)	+0.883(32)	-0.052(22)
$\tilde{b}_P - \tilde{b}_A$	Eq.(31)	-0.079(54)	-0.031(74)
$\tilde{b}_S - \tilde{b}_V - 2(\tilde{b}_P - \tilde{b}_A)$	Eq.(32)	-0.331(201)	+0.112(338)

TABLE IV: Results for the **60NPf** data set.

dominated by the pion, contributions proportional to $aB_\pi \equiv aM_\pi^2/2\tilde{m}$, while formally of $O(a\Lambda_{\text{QCD}})$, can be numerically much larger. These cases are discussed in more detail in the following sections.

Given these estimates of the uncertainties, we find that, at $\beta = 6.2$, there is complete consistency between our results and those from the ALPHA collaboration. Indeed, the only statistically significant difference is for Z_V^0 , which is calculated very precisely, but this difference is consistent with being an $\sim a^2\Lambda_{\text{QCD}}^2$ effect.

Moving to $\beta = 6$, we see that there are statistically significant differences not only for Z_V^0 , but also for c_A and c_V . For Z_V^0 the differences are consistent with the estimates of discretization errors given above. The difference for c_V (c_A) is about two (three) times the expected size of ~ 0.15 —this could be an enhanced $O(a)$ correction or an effect of higher order in a . Either way, what is clear is that, within $O(a)$ improvement, non-perturbative estimates of the c_X have substantial uncertainties at $\beta = 6$. The only definite conclusion that we can draw is that the c_X , which are zero at tree level, are small.

We find that the various constants show a strong dependence on the value of c_{SW} . The relatively small change from the non-perturbative value at $\beta = 6$ to the tadpole-improved value leads to noticeable changes in most of the constants.

One of the most surprising results of Ref. 8 was the large magnitude of $\tilde{b}_V - \tilde{b}_A \approx 0.5$ at

	reference	2-point	3-point
c_A	Eq.(15)	-0.036(05)	-0.043(08)
Z_V^0	Eq.(17)	+0.770(01)	+0.769(01)
\tilde{b}_V	Eq.(17)	+1.424(17)	+1.464(23)
Z_V^0	Eq.(17)	+0.769(01)	+0.768(01)
b_V	Eq.(17)	+1.522(11)	+1.523(11)
$Z_P^0/Z_A^0 Z_S^0$	Eq.(18,19)	+1.068(10)	+1.041(14)
Z_V^0	Eq.(22)	+0.766(04)	+0.766(04)
$\tilde{b}_A - \tilde{b}_V$	Eq.(22)	-0.288(43)	-0.256(53)
Z_V^0	Eq.(22)	+0.768(04)	+0.768(04)
$b_A - b_V$	Eq.(22)	-0.267(40)	-0.236(50)
$Z_V^0/(Z_A^0)^2$	Eq.(25)	+1.204(11)	+1.194(13)
$\tilde{b}_A - \tilde{b}_V$	Eq.(25)	+0.007(106)	+0.043(126)
Z_A^0	Eq.(20,25)	+0.806(04)	+0.797(04)
$Z_P^0/Z_A^0 Z_S^0$	Eq.(26)	+1.061(10)	+1.050(14)
$Z_P^0/Z_A^0 Z_S^0$	Eq.(27)	+1.051(08)	+1.027(12)
$\tilde{b}_P - \tilde{b}_S$	Eq.(26)	-0.114(44)	-0.097(44)
c_T	Eq.(30)	+0.057(10)	+0.084(13)
$\tilde{b}_A - \tilde{b}_P + \tilde{b}_S/2 [c_A(m)]$	Eq.(27)	+0.596(33)	+0.547(58)
$\tilde{b}_A - \tilde{b}_P + \tilde{b}_S/2 [c_A(0)]$	Eq.(27)	+0.881(33)	-0.051(23)
$\tilde{b}_P - \tilde{b}_A$	Eq.(31)	-0.058(54)	+0.002(81)
$\tilde{b}_S - \tilde{b}_V - 2(\tilde{b}_P - \tilde{b}_A)$	Eq.(32)	-0.379(247)	+0.096(439)

TABLE V: Results for the **60NPb** data set.

$\beta = 6$ with tadpole-improved c_{SW} . This difference is predicted to be very small (0.002) in 1-loop perturbation theory, and even assuming the 2-loop term to be $\sim \alpha_s^2$ suggests a much smaller value ≈ 0.02 (0.015) at $\beta = 6$ (6.2). We find that the measured difference is reduced to ~ 0.3 using the non-perturbative c_{SW} , and further reduced to ~ 0.1 at $\beta = 6.2$. While the latter difference is small enough to be accounted for by the expected $a\Lambda_{QCD}$ uncertainty, the larger result at $\beta = 6$ may indicate higher order uncertainties.

The other differences between \tilde{b} 's are more stable, and are consistent with perturbative predictions within the $O(a)$ uncertainties. The same is true of our final results for the \tilde{b} 's themselves; the largest difference is for \tilde{b}_V and is $\sim 2a\Lambda_{QCD}$.

In fact, allowing for $(1-2)a\Lambda_{QCD}$ discretization uncertainties, the only non-perturbative result which is in disagreement with perturbation theory is Z_P^0/Z_S^0 . A very large two loop effect, $\sim -4\alpha^2$, is required to bring the results into agreement. This finding is consistent with those of the APE collaboration who argue that $Z_P - 1$ is significantly underestimated by 1-loop perturbation theory [19].

Concerning the statistical errors, we see a substantial improvement in the signal between $\beta = 6.0$ and 6.2. It is also noteworthy that the errors in our estimates are comparable to those from the ALPHA collaboration. While a precise comparison of efficacies is difficult

	reference	2-point	3-point
c_A	Eq.(15)	-0.032(03)	-0.038(04)
Z_V^0	Eq.(17)	+0.787(00)	+0.787(00)
\tilde{b}_V	Eq.(17)	+1.304(10)	+1.312(10)
Z_V^0	Eq.(17)	+0.787(00)	+0.787(00)
b_V	Eq.(17)	+1.422(08)	+1.422(08)
$Z_P^0/Z_A^0 Z_S^0$	Eq.(18,19)	+1.091(05)	+1.084(05)
Z_V^0	Eq.(22)	+0.788(02)	+0.790(02)
$\tilde{b}_A - \tilde{b}_V$	Eq.(22)	-0.111(27)	-0.071(28)
Z_V^0	Eq.(22)	+0.788(02)	+0.791(02)
$b_A - b_V$	Eq.(22)	-0.109(26)	-0.071(27)
$Z_V^0/(Z_A^0)^2$	Eq.(25)	+1.185(04)	+1.181(05)
$\tilde{b}_A - \tilde{b}_V$	Eq.(25)	-0.092(62)	-0.115(59)
Z_A^0	Eq.(20,25)	+0.818(02)	+0.813(02)
$Z_P^0/Z_A^0 Z_S^0$	Eq.(26)	+1.085(04)	+1.077(05)
$Z_P^0/Z_A^0 Z_S^0$	Eq.(27)	+1.077(05)	+1.071(05)
$\tilde{b}_P - \tilde{b}_S$	Eq.(26)	-0.086(23)	-0.075(23)
c_T	Eq.(30)	+0.051(07)	+0.078(07)
$\tilde{b}_A - \tilde{b}_P + \tilde{b}_S/2 [c_A(m)]$	Eq.(27)	+0.626(24)	+0.619(29)
$\tilde{b}_A - \tilde{b}_P + \tilde{b}_S/2 [c_A(0)]$	Eq.(27)	+0.850(19)	+0.123(17)
$\tilde{b}_P - \tilde{b}_A$	Eq.(31)	-0.086(26)	-0.062(34)
$\tilde{b}_S - \tilde{b}_V - 2(\tilde{b}_P - \tilde{b}_A)$	Eq.(32)	+0.047(106)	+0.176(137)

TABLE VI: Results for the **62NP** data set.

because of different systematic errors, and different ensemble and lattice sizes, we conclude that our method is competitive.

V. CALCULATION OF c_A

The determination of c_A is central to the extraction of all quantities that are obtained using the axial Ward identity Eq. (10) since c_A enters in $\delta\mathcal{S}$ [see Eq. (6)]. Its evaluation uses the AWI with no operator present in the domain of chiral rotation. In particular, c_A is adjusted so that the ratio

$$\frac{\sum_{\vec{x}} \langle \partial_\mu [A_\mu + ac_A \partial_\mu P]^{(ij)}(\vec{x}, t) J^{(ji)}(0) \rangle}{\sum_{\vec{x}} \langle P^{(ij)}(\vec{x}, t) J^{(ji)}(0) \rangle} = 2\tilde{m}_{ij}, \quad (15)$$

which defines the quark mass \tilde{m}_{ij} , is independent of the source J and the time t at which it is evaluated. Since this criterion is automatically satisfied when the correlators are saturated by a single state, the determination of c_A relies on the behavior of excited state contributions at small t .

62NP				
	2pt		3pt	
	$c_A(m)$	$c_A(0)$	$c_A(m)$	$c_A(0)$
extrap.	-0.115(63)	-0.087(62)	-0.032(64)	-0.096(61)
$1/m$ fit	-0.086(15)	-0.102(17)	-0.172(20)	-0.123(19)
slope ratio	-0.094(19)	-0.094(19)	-0.107(19)	-0.109(19)
60NPf				
	2pt		3pt	
	$c_A(m)$	$c_A(0)$	$c_A(m)$	$c_A(0)$
extrap.	-0.094(56)	-0.060(57)	+0.046(68)	-0.048(63)
$1/m$ fit	-0.131(26)	-0.205(38)	-0.363(71)	-0.209(53)
slope ratio	-0.116(19)	-0.116(19)	-0.113(26)	-0.120(26)
60NPb				
	2pt		3pt	
	$c_A(m)$	$c_A(0)$	$c_A(m)$	$c_A(0)$
extrap.	-0.119(78)	-0.086(78)	+0.013(87)	-0.067(81)
$1/m$ fit	-0.071(38)	-0.157(45)	-0.359(86)	-0.171(63)
slope ratio	-0.097(30)	-0.096(31)	-0.092(37)	-0.102(37)
60TI				
	2pt		3pt	
	$c_A(m)$	$c_A(0)$	$c_A(m)$	$c_A(0)$
extrap.	-0.483(124)	-0.468(125)	-0.337(135)	-0.451(131)
$1/m$ fit	-0.143(63)	-0.162(65)	-0.367(80)	-0.158(71)
slope ratio	-0.253(48)	-0.252(49)	-0.222(53)	-0.244(55)

TABLE VII: Results for c_V . See text (sec. VII) for details.

To implement Eq. (15) one has to choose how to discretize the derivatives. Note that all choices lead to the same improvement and normalization constants at the order we are working, *i.e.* up to $O(a)$ and $O(a^2)$ errors, respectively. This is because the difference between discretizations is explicitly proportional to a^2 . Thus investigating the sensitivity to the choice of discretization gives information on the size of higher order discretization errors.

We limit our study of this issue to the comparison between two discretization schemes. Both are based on a mixture of 2-point and 3-point discretizations. This terminology is explained in Ref. 8, and is exemplified by $\partial_x f(x + 0.5) \rightarrow (f(x + 1) - f(x))/a$ (2-point) and $\partial_x f(x) \rightarrow (f(x + 1) - f(x - 1))/2a$ (3-point). Results from both schemes are quoted in Tabs. III, IV, V and VI.

In our first scheme, we implement Eq. (15) using 2-point discretization. In the subsequent calculations, based on the AWI of Eq. (10) we use the same 2-point discretization in δS [Eq. (6)] as in Eq. (15), and replace the continuum integral by a simple sum. For the derivatives within the operators \mathcal{O} and $\delta\mathcal{O}$, however, we use 3-point discretization. In our second scheme, we repeat the calculations using the value of c_A obtained when enforcing Eq. (15) with a 3-point discretization for the derivatives. The remainder of the calculation is done with the same discretizations for δS , \mathcal{O} and $\delta\mathcal{O}$ as in the 2-point scheme but the new value for c_A .

There is a subtlety in the comparison between results from the two schemes. It follows

	$\beta = 6.0$				$\beta = 6.2$		
	LANL	LANL	ALPHA	P. Th.	LANL	ALPHA	P. Th.
c_{SW}	1.4755	1.769	1.769	1.521	1.614	1.614	1.481
Z_V^0	+0.747(1)	+0.770(1)	0.7809(6)	+0.810	+0.7874(4)	+0.7922(4)(9)	+0.821
Z_A^0	+0.791(7)(4)	+0.807(2)(8)	0.7906(94)	+0.829	+0.818(2)(5)	+0.807(8)(2)	+0.839
Z_P^0/Z_S^0	+0.811(9)(5)	+0.842(5)(1)	N.A.	+0.956	+0.884(3)(1)	N.A.	+0.959
c_A	-0.022(6)(1)	-0.037(4)(8)	-0.083(5)	-0.013	-0.032(3)(6)	-0.038(4)	-0.012
c_V	-0.25(5)(3)	-0.107(17)(4)	-0.32(7)	-0.028	-0.09(2)(1)	-0.21(7)	-0.026
c_T	+0.09(2)(1)	+0.06(1)(3)	N.A.	+0.020	+0.051(7)(17)	N.A.	+0.019
\tilde{b}_V	+1.44(3)(2)	+1.43(1)(4)	N.A.	+1.106	+1.30(1)(1)	N.A.	+1.099
b_V	+1.53(2)	+1.52(1)	+1.54(2)	+1.274	+1.42(1)	+1.41(2)	+1.255
$\tilde{b}_A - \tilde{b}_V$	-0.51(9)(4)	-0.26(3)(4)	N.A.	-0.002	-0.11(3)(4)	N.A.	-0.002
$b_A - b_V$	-0.49(9)(4)	-0.24(3)(4)	N.A.	-0.002	-0.11(3)(4)	N.A.	-0.002
$\tilde{b}_P - \tilde{b}_S$	-0.07(9)(2)	-0.06(4)(3)	N.A.	-0.066	-0.09(2)(1)	N.A.	-0.062
$\tilde{b}_P - \tilde{b}_A$	-0.126(58)(1)	-0.07(4)(5)	N.A.	+0.002	-0.09(3)(3)	N.A.	+0.001
\tilde{b}_A	+0.92(10)(6)	+1.17(4)(8)	N.A.	+1.104	+1.19(3)(5)	N.A.	+1.097
b_A	+1.05(9)(4)	+1.28(3)(4)	N.A.	+1.271	+1.32(3)(4)	N.A.	+1.252
\tilde{b}_P	+0.80(11)(6)	+1.10(5)(13)	N.A.	+1.105	+1.11(4)(7)	N.A.	+1.099
\tilde{b}_S	+0.87(14)(4)	+1.16(6)(11)	N.A.	+1.172	+1.19(4)(6)	N.A.	+1.161

TABLE VIII: Final results for improvement and renormalization constants. The first error is statistical, and the second, where present, corresponds to the difference between using 2-point and 3-point discretization of the derivative used in the extraction of c_A .

from the relation

$$\begin{aligned}
& \langle \partial_\mu [(A_I^{(2\text{-point})})_\mu(c_A) - 2mP^{(2\text{-point})}](t + a/2)J(0) \rangle + \\
& \langle \partial_\mu [(A_I^{(2\text{-point})})_\mu(c_A) - 2mP^{(2\text{-point})}](t - a/2)J(0) \rangle = \\
& 2\langle \partial_\mu [(A_I^{(3\text{-point})})_\mu(c_A - am/2) - 2mP](t)J(0) \rangle + O(a^3). \tag{16}
\end{aligned}$$

that the $O(a^2)$ differences between 2-point and 3-point discretizations can be absorbed by shifting $c_A \rightarrow c_A - am/2$ in the latter scheme. Thus, if one were to fit to the same range of timeslices with appropriate weights, as defined by Eq. (16), the difference between c_A from 2-point and 3-point determinations would be of $O(a^2)$ in the chiral limit. This difference would then not be useful as an indicator of $O(a)$ discretization errors.

In practice, however, our fits do not weight the points appropriately for the relation (16) to be relevant. In particular, we find that using the 2-point scheme, the best fits are for $t \geq 2$ relative to the source at $t = 0$, where $t = 2$ (which corresponds to evaluating the derivative at $t = 2.5$) is the earliest timeslice at which there are no contact terms for either discretization scheme. On the other hand, for the 3-point scheme, we are not able to include the point at $t = 2$ as the $O(a^2)$ errors are too large and the fit has poor quality (this was checked by turning on the full covariance matrix). Because of this, the resulting values of c_A do differ at $O(a)$, and we take this the difference as an estimate of the size of the higher order discretization errors.

	60TI	60NPf	60NPb	62NP
$c'_V + c'_P$	+2.75(23)	+2.82(15)	+2.68(19)	+2.62(8)
$c'_A + c'_P$	+2.30(46)	+2.43(24)	+2.12(31)	+2.43(14)
$2c'_P$	-1.96(152)	+0.88(97)	-0.65(57)	+1.82(24)
$c'_S + c'_P$	+2.02(21)	+2.44(13)	+2.40(13)	+2.40(7)
$c'_T + c'_P$	+2.26(33)	+2.40(18)	+2.27(20)	+2.42(9)
c'_V	+3.72(73)	+2.38(50)	+3.00(37)	+1.72(16)
c'_A	+3.28(94)	+1.99(56)	+2.45(46)	+1.53(20)
c'_P	-0.98(76)	+0.44(49)	-0.33(29)	+0.91(12)
c'_S	+3.00(73)	+2.00(48)	+2.72(33)	+1.49(14)
c'_T	+3.24(75)	+1.96(49)	+2.60(38)	+1.51(15)

TABLE IX: Results for off-shell mixing coefficients.

In our final compilation, Tab. VIII, the central values are from the 2-point approximation, while the difference between the two discretizations is quoted as a systematic error. We note that the ALPHA collaboration has used 3-point discretization of all derivatives. This does not, however, imply that their results should be more closely comparable to ours based on the c_A with 3-point discretization, since there are other differences in the calculations.

To use Eq. (15) we must also choose the source J . Different sources produce different admixtures of the ground and excited states, and thus have varying sensitivities for determining c_A . Furthermore, different sources give values for c_A differing by $O(a)$ (or $O(1)$ if the action is not fully $O(a)$ improved). We have investigated source dependence using results from a separate calculation performed on 170 quenched lattices of size $32^3 \times 64$ at $\beta = 6.0$ using the Wilson ($c_{SW} = 0$) [20] and tadpole-improved clover ($c_{SW} = 1.4785$) [21] actions. (The slightly different value of $c_{SW} = 1.4755$ used in the **60TI** calculation was an oversight.) The results from three different sources are shown in Fig. 2. The sources are $J = A_4$ and $J = P$, both with wall source smearing, and $J = P$ with Wuppertal smearing. We do not present the $J = A_4$ data with Wuppertal smearing as that correlator is dominated by the ground state already at $t \sim 4$, and is thus very insensitive to c_A . Results from the Wilson action depend substantially on the source, even in the chiral limit. This is as expected since the action is not improved, leading to large, $O(1)$, variations in c_A . Also, as expected, there is a marked convergence when using the tadpole-improved action. Indeed, results from the three sources are consistent within errors (and linear extrapolation to the chiral limit gives a result, $c_A = -0.026(2)$, consistent with our **60TI** result quoted in Tab. III), and have similar sensitivity in determining c_A . Because of this, we have chosen to use only $J = P$ with Wuppertal smearing in the simulations devoted to calculating improvement constants.

We illustrate our determination of c_A (with 2-point discretization) using the non-perturbatively improved action in Figs. 3 and 4. We tune c_A so as to extend the plateau to the earliest timeslice $t = 2$ at which there are no contact contributions (the source is at $t = 0$). We have enough sensitivity to clearly distinguish c_A from zero. At $\beta = 6$ we can also distinguish c_A from that obtained by the ALPHA collaboration for the chiral limit ($c_A = -0.083(5)$). This difference remains after we extrapolate our results to the chiral

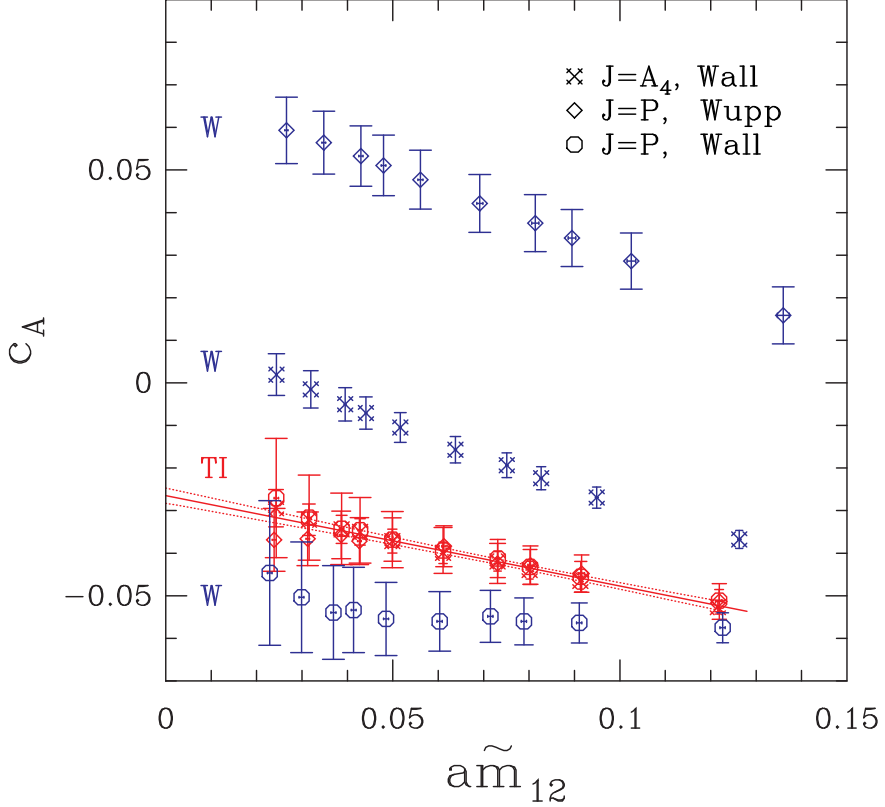


FIG. 2: Estimates of c_A versus the quark mass for three different sources J as discussed in the text. For the Wilson action (W), estimates of c_A from the three J are very different. The improvement in going to the tadpole-improved clover action (TI) is dramatic, and the three sets of data collapse together. We show a linear fit to this combined tadpole-improved clover data.

limit (giving $c_A = -0.037(4)$ ³ for the two-point discretization and $c_A = 0.045(7)$ for the three-point discretization). At $\beta = 6.2$ our results for c_A differ from the ALPHA value, $c_A = -0.038(4)$, at non-zero quark mass (as shown in the Figs. 4 and 5), but after chiral extrapolation they are consistent with the ALPHA result. This extrapolation (which is done using a linear fit to the masses $\kappa_2 - \kappa_5$) is shown in Fig. 5.

In our previous paper [8] we used tadpole-improved fermions at $\beta = 6$, and found a result inconsistent with that of the ALPHA collaboration, as can be seen from Tab. VIII. We did not, however, have enough information to determine the source of this difference. Our new result shows that while increasing c_{SW} to its non-perturbative value moves c_A towards the ALPHA result, a significant difference of ~ 0.046 remains. This difference is presumably due to higher order discretization errors. It is striking, however, that the difference is reduced substantially by changing β from 6.0 to 6.2. Since a^2 only halves between $\beta = 6$ and 6.2, this suggests that even higher order discretization errors are playing a dominant role. By contrast, the reduction in the difference between our results for 2- and 3-point discretizations

³ The difference in c_A in the **60NPf** and **60NPb** estimates is due only to the different number of configurations analyzed. Since the **60NPb** sample is a subset of **60NPf**, we quote the **60NPf** result as our best estimate

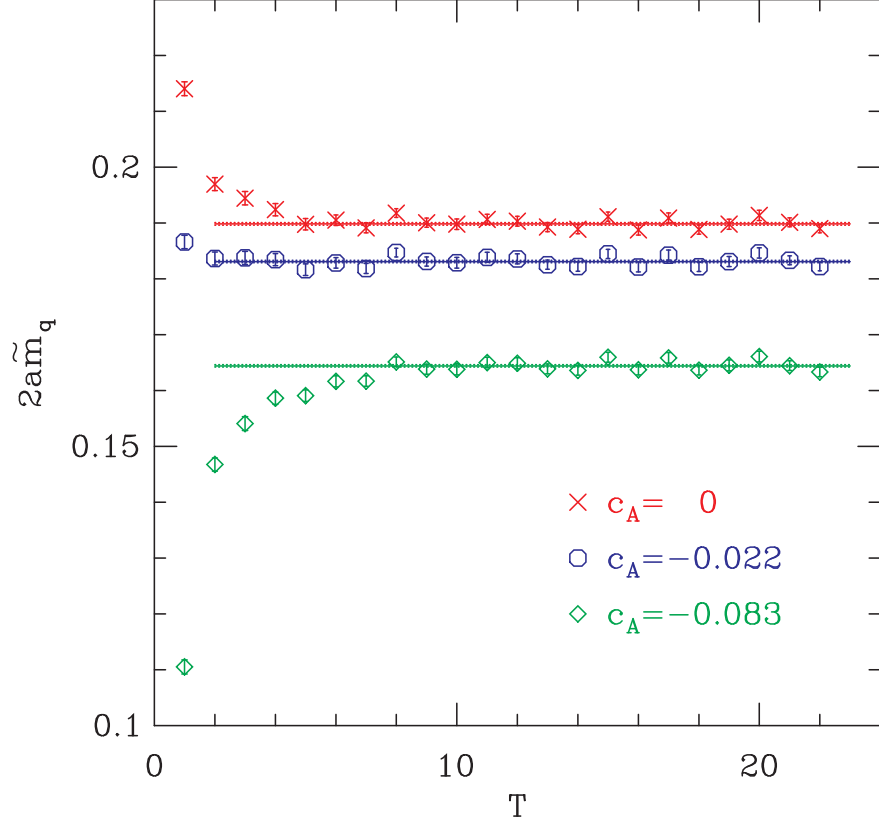


FIG. 3: Estimates of $2\tilde{m}_{ij}$ for different values of c_A illustrated using $i = j = \kappa_3$ in the **60NPf** data set and 2-point discretization. For this value of quark mass, setting $c_A = -0.022$ extends the plateau to the earliest time slice $t = 2$ at which there are no contact contributions. The fit for $c_A = -0.083$, the value obtained by the ALPHA collaboration in the chiral limit, and $c_A = 0$ are included to illustrate sensitivity.

is consistent with being an a^2 effect.

It is interesting to compare our non-perturbative results for c_A with perturbative estimates. We see from Tab. VIII that the 1-loop result ($\sim 0.2 \times \alpha$) gives a substantial underestimate. To explain the difference one needs a large two-loop term, $\sim \alpha^2$, which, using the values quoted in Appendix A, is 0.018 and 0.016 for $\beta = 6$ and 6.2, respectively.

We close with a comment on the practical implementation of the AWI. To the accuracy we are working, we can use, in δS , either the appropriate mass-dependent c_A or its value in the chiral limit. We prefer the former, and use it throughout, because it maintains the relation $\partial_\mu (A_I)_\mu^{(ij)} - 2\tilde{m}_{ij} P^{(ij)} = 0$ at finite quark masses on the states used to tune c_A . Our data suggest that this relation receives only small corrections on other states relevant to the AWI. This ensures (for the c_A obtained using 2-point derivatives) that the ratio in Eq. (10) is nearly independent of the time slice of the insertion of the improved operator and the volume V of chiral rotation. We stress, however, that when the axial current appears as an operator in the AWI, we use the chirally extrapolated c_A to give our central values (see Section II), and use the mass-dependent c_A to give an indication of the size of higher order discretization errors.

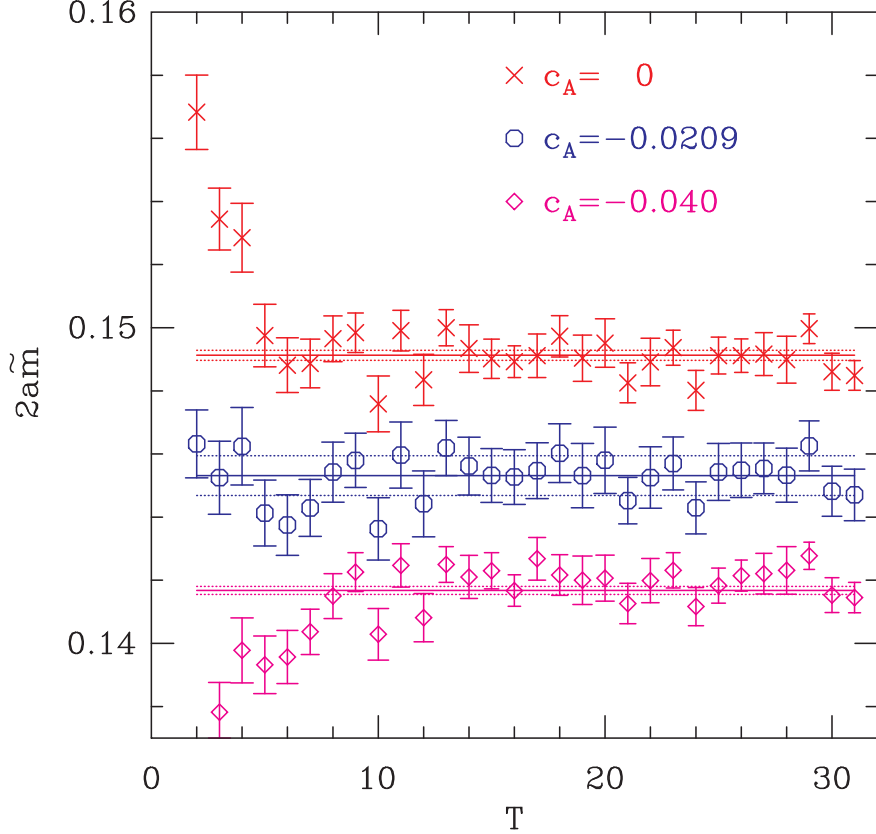


FIG. 4: Estimates of $2\tilde{m}_{ij}$ for different values of c_A illustrated using $i = j = \kappa_3$ and the **62NP** data set. For this quark mass, $c_A = -0.0209$ extends the plateau to the earliest allowed time slice $t = 2$. To show sensitivity to the tuning we contrast this best fit with those using $c_A = 0$ and $c_A = -0.040$.

VI. Z_V^0 AND b_V

The matrix elements of the vector charge $\int d^3x V_4^{(23)}(x)$, with $m_2 = m_3$, are fixed by the charge of the states, and allow a determination of Z_V as a function of the quark mass. Our best signal is for the matrix element between pseudoscalar mesons:

$$\frac{1}{Z_V^0(1 + \tilde{b}_V a \tilde{m}_2)} = \frac{\sum_{\vec{x}, \vec{y}} \langle P^{(12)}(\vec{x}, \tau) (V_I)_4^{(23)}(\vec{y}, t) J^{(31)}(0) \rangle}{\langle \sum_{\vec{x}} P^{(12)}(\vec{x}, \tau) J^{(21)}(0) \rangle}. \quad (17)$$

with $\tau > t > 0$ and $J = P$ or A_4 . The two sources have comparable signal, and the final results are obtained by averaging the two estimates when constructing the jackknife ensemble. Note that the $O(a)$ improvement term in V_I does not contribute. Z_V^0 and \tilde{b}_V are then extracted by fitting the data as a function of \tilde{m}_2 .

As an illustration we describe the procedure for the **62NP** data set. The quality of the data is very good, as shown in Fig. 6. A linear fit is clearly inadequate, so we use a quadratic fit

$$Z_V = 0.7874(4) [1 + 1.304(10) \tilde{m}_2 a + 1.062(52) (\tilde{m}_2 a)^2]. \quad (18)$$

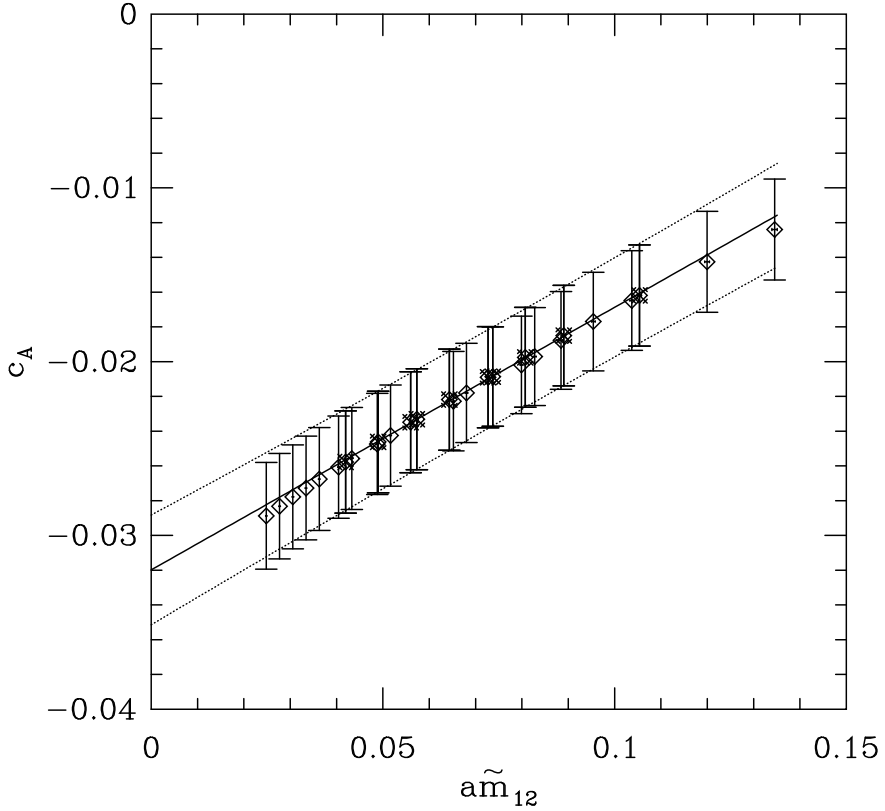


FIG. 5: The chiral extrapolation of c_A for **62NP** data. Diamonds label all mass combinations and stars highlight the ten combinations of $\kappa_2 - \kappa_5$ used in the fit.

The intercept is our result for Z_V^0 , while the coefficient of the linear term, *i.e.* the slope in the chiral limit, is our result for b_V . Note that if we had simply used a linear fit over our mass range, the result for b_V would have been 1.469(9), in complete disagreement with our quoted result.

We can also fit Z_V as a function of $m = 1/2\kappa - 1/2\kappa_c$. This provides a consistency check for Z_V^0 , and a direct determination of b_V . The fit gives

$$Z_V = 0.7871(3) [1 + 1.422(8)ma + 0.05(4)(ma)^2]. \quad (19)$$

In this case the quadratic term is small. The intercept is consistent, at the 2σ level, with that from Eq. (18). We can use these two fits to also extract the combination $(Z_P^0/Z_A^0 Z_S^0)$ from the ratio of the coefficients of the linear term as explained in Sec. IX. The results are given in Tabs. III–VI, and are consistent with those obtained from the axial Ward identity, Eq. (26), even though the $O(a^2)$ errors could have been different in the two methods.

Our results for Z_V^0 and b_V are compared with those from the ALPHA collaboration in Tab. VIII. There are small differences for Z_V^0 , 0.011(1) and 0.005(1), respectively, at $\beta = 6.0$ and 6.2. These are of the expected magnitude for $O(a^2)$ differences, and are consistent with $O(a^2)$ scaling. The results for b_V are, on the other hand, already consistent.

The difference between 1-loop tadpole-improved perturbation theory and our non-perturbative Z_V^0 is 0.040(1) at $\beta = 6.0$ and 0.034(1) at $\beta = 6.2$, where only statistical errors have been considered. Recall that the discretization errors are expected to be of

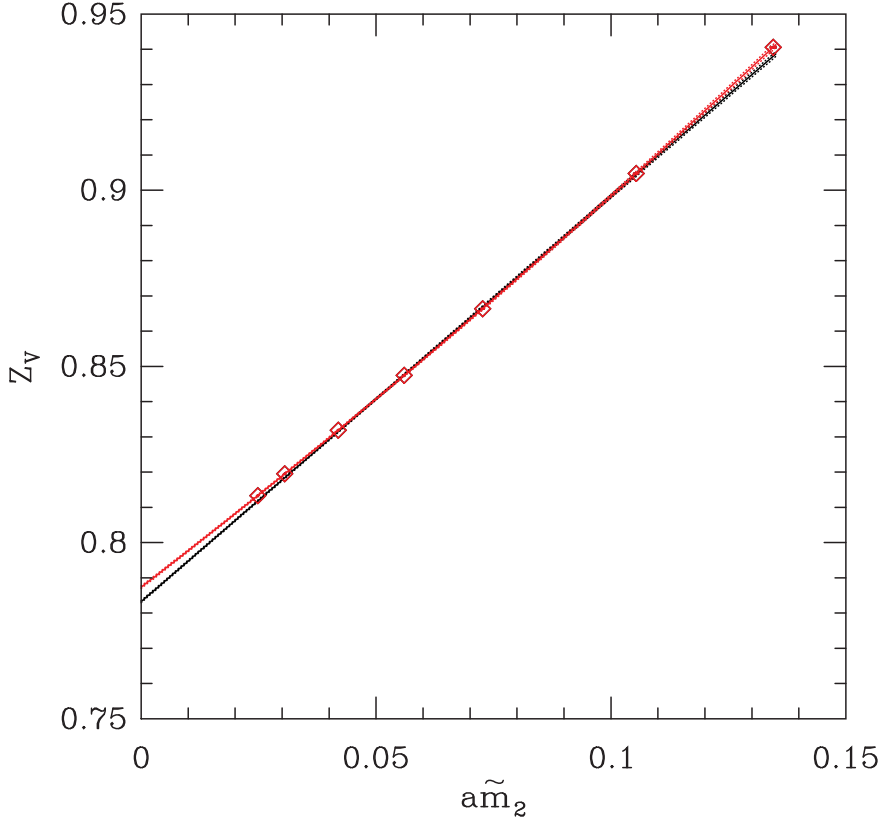


FIG. 6: Linear and quadratic fit to Z_V versus \tilde{m}_2 for the **62NP** data set.

size $(a\Lambda_{\text{QCD}})^2 \approx 0.02$ and 0.01 , respectively, while the missing two loop perturbative terms should be $\sim \alpha_s^2 \approx 0.02$ and 0.016 , respectively. Thus the deviation from perturbation theory is of the expected size, and the scaling behavior is closer to $O(\alpha_s^2)$ than to $O(a^2)$. The numerical values are consistent with $\approx 2\alpha_s^2$.

The non-perturbative results for b_V exceed the 1-loop estimates by $0.24(2)$ and $0.16(2)$, respectively, at the two couplings. These differences are much larger than the missing two-loop contributions, but are consistent with a discretization error of size $\approx 1.5a\Lambda_{\text{QCD}}$.

Results for Z_V are needed to calculate the vector decay constants and semi-leptonic form factors of D and B mesons. Note that, at $\beta = 6.2$, the charm and bottom quark masses are, in lattice units, roughly 0.5 and 2.0 , respectively, to be compared to our largest mass of 0.13 . It is thus important to ascertain to what mass the fits, given in Eqs. (18) and (19), can be used reliably. To address this issue we show in Fig. 7 how the two fits extend to higher quark masses for $\beta = 6.2$. A plot of the quantity m/\tilde{m} [Eq. (27)] which we use to convert $\tilde{m}a$ to ma is also included. We also show the recent non-perturbative results for Z_V obtained by the UKQCD collaboration [22]. Comparing our fits with the UKQCD data we find that both fits provide reliable estimates (to within 2%) up to the charm quark mass, with the fit to Eq. (18) being slightly better. In fact, over the range $0 \leq ma \lesssim 0.5$, truncating Eq. (19) at the linear order fits the UKQCD data to within 1% as already noted by them. Beyond $ma \approx 0.5$ the two fits start to deviate, and their validity near the bottom quark mass needs to be examined.

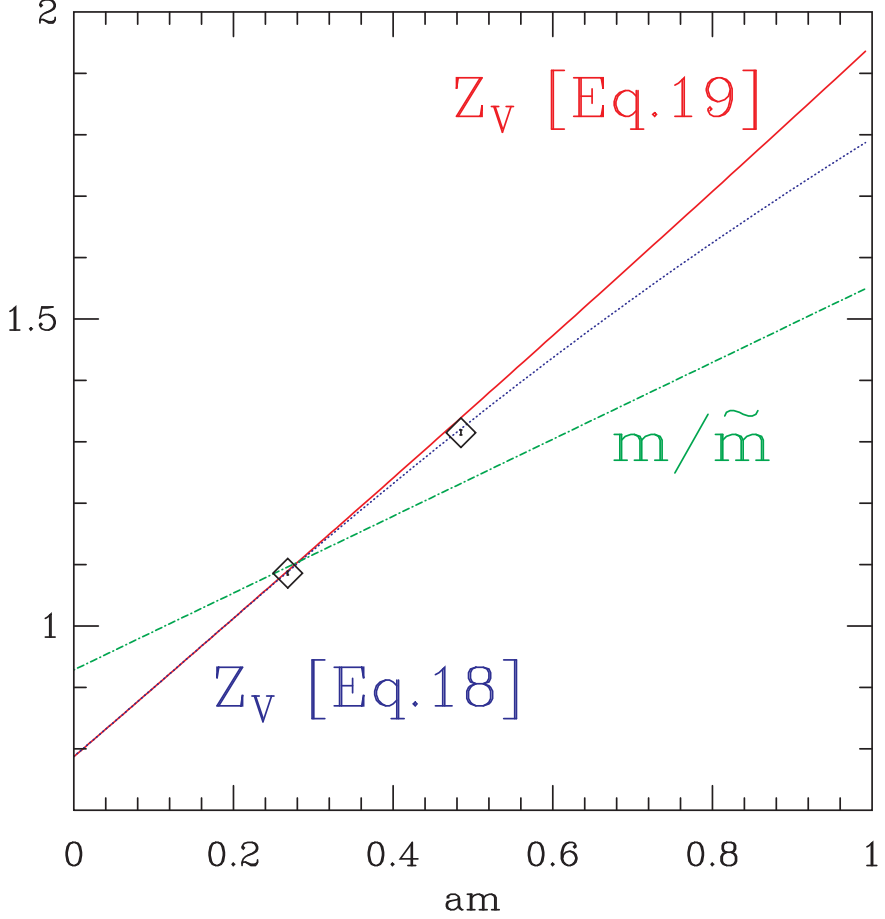


FIG. 7: Predictions for Z_V at $\beta = 6.2$ obtained by extending our fits, eqs. (18) and (19), to larger quark masses. The result for m/\tilde{m} is also shown, as are data points from the UKQCD collaboration.

VII. c_V AND $\tilde{b}_A - \tilde{b}_V$

We now turn to the analyses of the various 3-point axial Ward identities, and first consider the determination of the improvement coefficient c_V . A precise determination of c_V is important both for phenomenological applications and because the uncertainty in c_V contributes significantly to errors in Z_A^0 , Z_P^0/Z_S^0 , c_T , and c'_A . We have investigated several methods, and obtain the best results by enforcing

$$\frac{\sum_{\vec{y}} \langle \delta S_I^{(12)} (V_I)_4^{(23)}(\vec{y}, y_4) P^{(31)}(0) \rangle}{\sum_{\vec{y}} \langle (A_I)_4^{(13)}(\vec{y}, y_4) P^{(31)}(0) \rangle} = \frac{\sum_{\vec{y}} \langle \delta S_I^{(12)} [V_i + ac_V \partial_\mu T_{i\mu}]^{(23)}(\vec{y}, y_4) A_i^{(31)}(0) \rangle}{\sum_{\vec{y}} \langle (A_I)_i^{(13)}(\vec{y}, y_4) A_i^{(31)}(0) \rangle}, \quad (20)$$

where the dependence on c_V enters only on the r.h.s.. We emphasize two important features of this method. First, it does not require knowledge of the normalization constants Z_A and Z_V , since these appear in the same combination on both sides of Eq. (20). Second, the relation holds for any value of the quark masses, since the contact terms are the same on both sides [see Eq. (10)]. The determination of c_V does, however, require knowledge of c_A , which enters both in δS and in $(A_I)_4^{(13)}$ on the l.h.s..

The two correlators on the l.h.s. are dominated by the pion channel and the signal is excellent in the individual correlators as well as in the ratio. The latter is illustrated in Fig. 8. On the other hand, the correlators on the r.h.s. are dominated by the a_1 intermediate state, for which the signal is not as good. We illustrate this by showing, in Figs. 9 and 10, the terms independent of and proportional to c_V . It turns out that the difference between the l.h.s. and the c_V independent term on the r.h.s. is about 2% of the individual terms, and is comparable to the error, which is dominated by that from the term on the r.h.s.. Nevertheless, as explained below, we can extract c_V with reasonable precision. To do this it is convenient to rewrite Eq. (20) in terms of the following two quantities:

$$N = \frac{\sum_{\vec{y}} \langle \delta \mathcal{S}_I^{(12)} (V_I)_4^{(23)}(\vec{y}, y_4) J^{(31)}(0) \rangle}{\sum_{\vec{y}} \langle (A_I)_4^{(13)}(\vec{y}, y_4) J^{(31)}(0) \rangle} - \frac{\sum_{\vec{y}} \langle \delta \mathcal{S}_I^{(12)} V_i^{(23)}(\vec{y}, y_4) A_i^{(31)}(0) \rangle}{\sum_{\vec{y}} \langle (A_I)_i^{(13)}(\vec{y}, y_4) A_i^{(31)}(0) \rangle},$$

$$D = \frac{\sum_{\vec{y}} \langle \delta \mathcal{S}_I^{(12)} a \partial_\mu T_{i\mu}^{(23)}(\vec{y}, y_4) A_i^{(31)}(0) \rangle}{\sum_{\vec{y}} \langle (A_I)_i^{(13)}(\vec{y}, y_4) A_i^{(31)}(0) \rangle}. \quad (21)$$

such that $c_V = N/D$.

The data exhibit three interesting features:

- Both N and D are, to a good approximation, linear in $\tilde{m}_1 - \tilde{m}_3$, as illustrated in Fig. 11 (N shows a weak dependence on $\tilde{m}_3 + \tilde{m}_1$ as well).
- Close to $\tilde{m}_1 = \tilde{m}_3$ both N and D vanish. However, since the discretization errors in N and D are different, they vanish at slightly different points. As a result the ratio N/D is very poorly determined when $\tilde{m}_1 = \tilde{m}_3$, and $c_V = N/D$ shows a spurious $1/(\tilde{m}_1 - \tilde{m}_3)$ singularity, as illustrated in Fig. 12.
- Estimates of c_V for the combination $\{\tilde{m}_i, \tilde{m}_j\}$ are highly anti-correlated with those for $\{\tilde{m}_j, \tilde{m}_i\}$. Estimates of c_V for $\tilde{m}_1 < \tilde{m}_3$ are consistently more negative as shown in Fig. 12.

Because of the spurious singularity mentioned above, we explore the following three approaches to determine c_V .

- Linearly extrapolate each of the three ratios of correlators to $\tilde{m}_1 = \tilde{m}_2 = 0$, working at fixed non-zero \tilde{m}_3 so as to avoid the singularity, and then solve for c_V . The weighted average over the different \tilde{m}_3 points is quoted in the first row in Tab. VII. This method yields estimates with the largest uncertainty, as illustrated in Fig. 13.
- Fit N/D to the form $c_V^{(0)} + c_V^{(1)}/(\tilde{m}_1 - \tilde{m}_3)$ (as illustrated in Fig. 12) and use $c_V = c_V^{(0)}$. We find that the result is insensitive to the range of quark masses used; the results quoted in Tab. VII are based on fits to $\kappa_2 - \kappa_5$ for **60TI** and **60NP** and $\kappa_1 - \kappa_6$ for **62NP**.
- Fit N and D separately to the form $\alpha + \gamma(\tilde{m}_1 - \tilde{m}_3)$, and take c_V to be the ratio of the slopes, γ_N/γ_D . This is legitimate since c_V is given, in principle, by N/D for all quark masses. This method avoids the use of the intercepts, α_N and α_D , which, being small, have larger discretization errors.

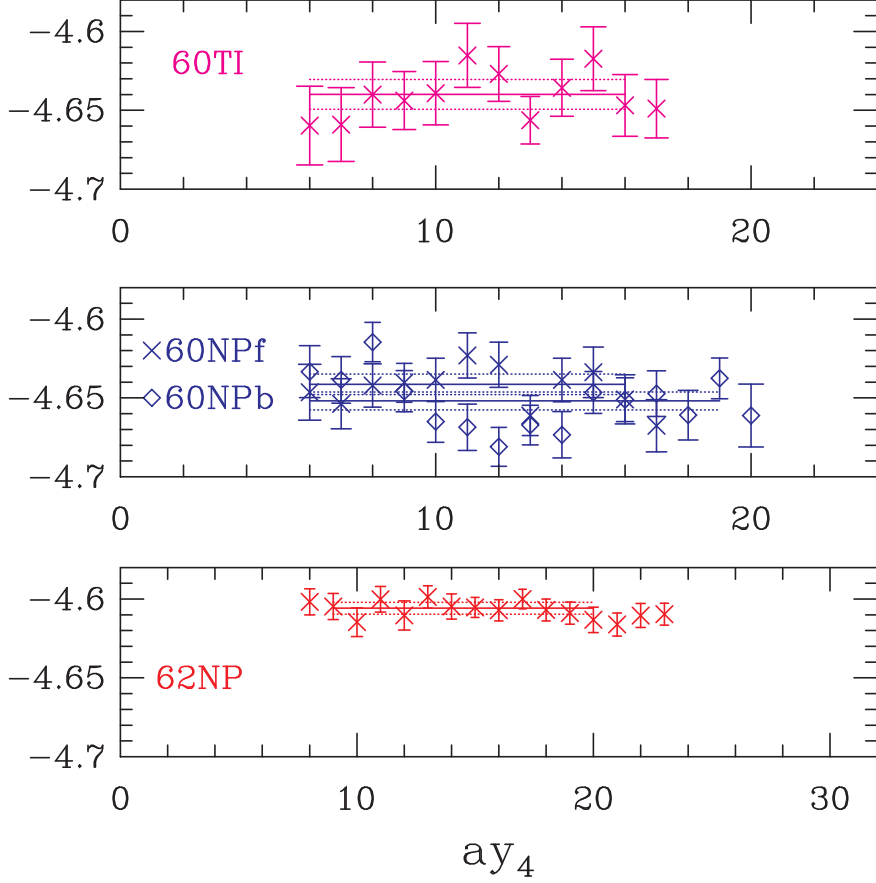


FIG. 8: Illustration of the quality of the signal for the l.h.s. of Eq. (20) for the four data sets. In all four cases all quark propagators correspond to κ_3 .

For each of these methods we evaluate c_V for four variants of c_A : for both the usual choices of 2-point versus 3-point discretization of $\partial_4 A_4$ when determining c_A using Eq. (15), we use mass dependent and chirally extrapolated values of c_A in the operator $(A_I)_4^{(13)}$ appearing in the denominator on the l.h.s. of Eq. (20).⁴ Results are quoted in Tab. VII. We find that only for the “slope-ratio” method do all four choices for c_A lead to consistent results. We also note that the estimates using all three methods are consistent if we use the 2-point c_A but not for the 3-point c_A . Thus we take for our best estimate the value obtained with the “slope-ratio” method and the 2-point (chirally extrapolated) c_A .

Our final results are collected in Tab. VIII. Our main conclusion is that c_V , which is zero at tree level, remains small in magnitude. We note that although our non-perturbative estimate is smaller than those of the ALPHA collaboration, the difference is consistent with being due to $a\Lambda_{\text{QCD}}$ corrections.

We have tried several other methods for determining c_V . One can demand that the r.h.s. of Eq. (20) be independent of y_4 . This turns out to be roughly true for the individual ratios, and thus holds independent of c_V . We have also tried different sources, *e.g.* $\mathcal{O} = A_i$, $J = V_i$ at zero momentum for the l.h.s. and $\mathcal{O} = A_4$, $J = V_4$ at non-zero momentum for the r.h.s.,

⁴ As noted in Sec. V, we always use the mass dependent c_A in δS .

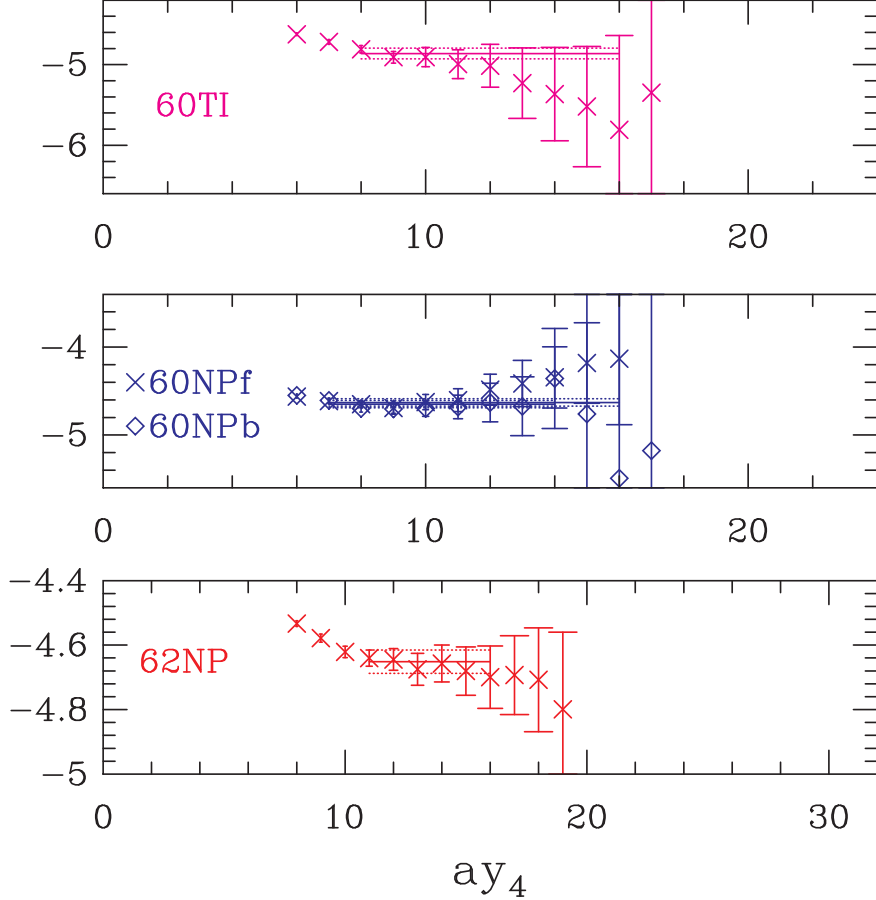


FIG. 9: Illustration of the quality of the signal for the first term on the r.h.s. of Eq. (20) for the four data sets. In all four cases all the quark propagators correspond to κ_3 .

making the intermediate state a vector meson. We have also implemented the method of the ALPHA collaboration 6, in which the l.h.s. with $\mathcal{O} = A_i, J = V_i$ at zero momentum is equated to unity in the chiral limit, making use of previously determined results for Z_A^0/Z_V^0 and Z_V^0 . In all the cases we have considered, however, the final estimates have larger errors than those quoted above. It is noteworthy, and perhaps surprising, that our best method involves an intermediate axial-vector state, rather than a vector meson.

The errors in our final result for c_V are substantially smaller than those of Ref. 6. It is likely that part of the explanation for this improvement is our use of a different AWI and fitting method.

To extract $\tilde{b}_A - \tilde{b}_V$ we use the l.h.s. of Eq. (20), so as to avoid dependence on c_V , and follow the procedure outlined in Sec. II. After extrapolating to $\tilde{m}_1 = \tilde{m}_2 = 0$, the ratio should be described by

$$\frac{Z_A^0(1 + \tilde{b}_A a \tilde{m}_3/2)}{Z_A^0 \cdot Z_V^0(1 + \tilde{b}_V a \tilde{m}_3/2)}. \quad (22)$$

The slope with respect to $\tilde{m}_3/2$ ($m_3/2$) gives our best estimate for $\tilde{b}_A - \tilde{b}_V$ ($b_A - b_V$) and the intercept gives a second estimate of Z_V^0 . As shown in Tabs. III-VI, the results for Z_V^0

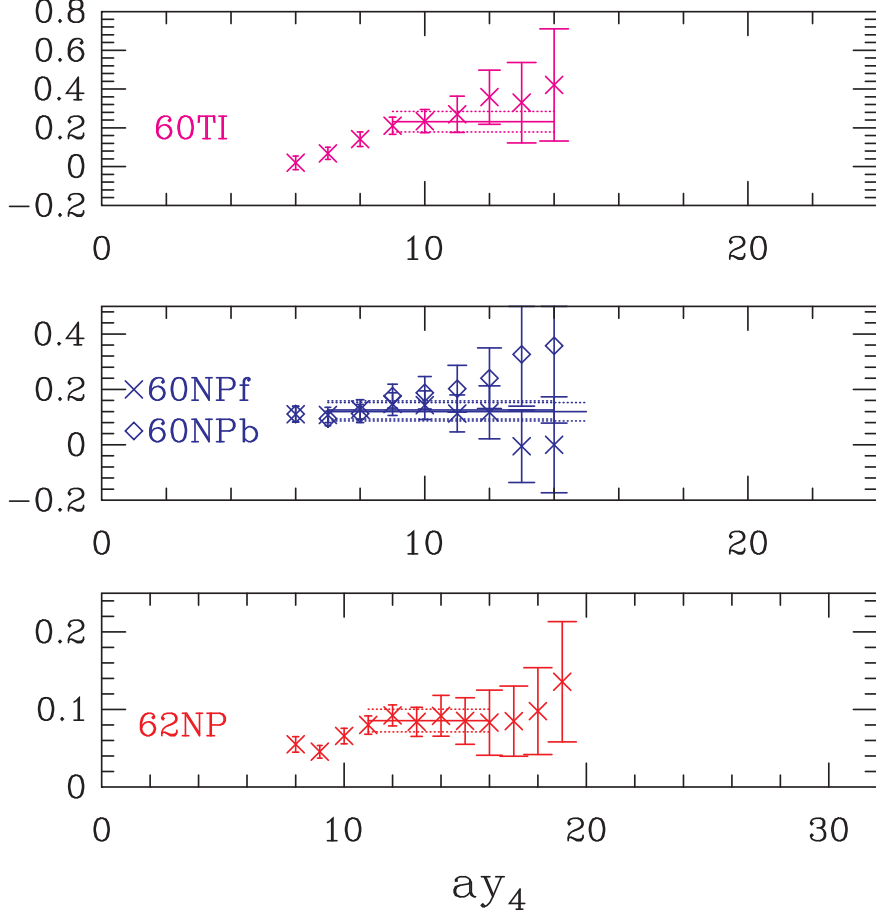


FIG. 10: Illustration of the quality of the signal for the ratio multiplying c_V in the r.h.s. of Eq. (20) for the four data sets, using κ_3 propagators in all cases.

are consistent with those from the VWI, but with somewhat larger errors. As an example of the fits, for the **62NP** data set we find

$$\begin{aligned} \frac{1 + (\tilde{b}_A - \tilde{b}_V)a\tilde{m}_3/2}{Z_V^0} &= 1.269(3)(1 - 0.111(27)a\tilde{m}_3/2) \\ \frac{1 + (b_A - b_V)am_3/2}{Z_V^0} &= 1.268(3)(1 - 0.109(26)am_3/2). \end{aligned} \quad (23)$$

The quality of the fits is shown in Fig. 14. Even though the intercept and the slope are almost identical, they are consistent with the expected relation $(\tilde{b}_A - \tilde{b}_V) = (Z_A^0 Z_S^0 / Z_P^0)(b_A - b_V) \approx 0.92(b_A - b_V)$ within the errors.

Since the correlators on the l.h.s. of Eq. (20) involve pion intermediate states, higher order discretization errors can be enhanced as noted in Sec. IV. For example, a change in the value of c_A used in the denominator, $\Delta c_A \sim a\Lambda_{QCD}$, leads to a change in Z_V^0 of size

$$\frac{\Delta Z_V^0}{Z_V^0} = \Delta c_A \frac{aM_\pi^2}{2\tilde{m}}. \quad (24)$$

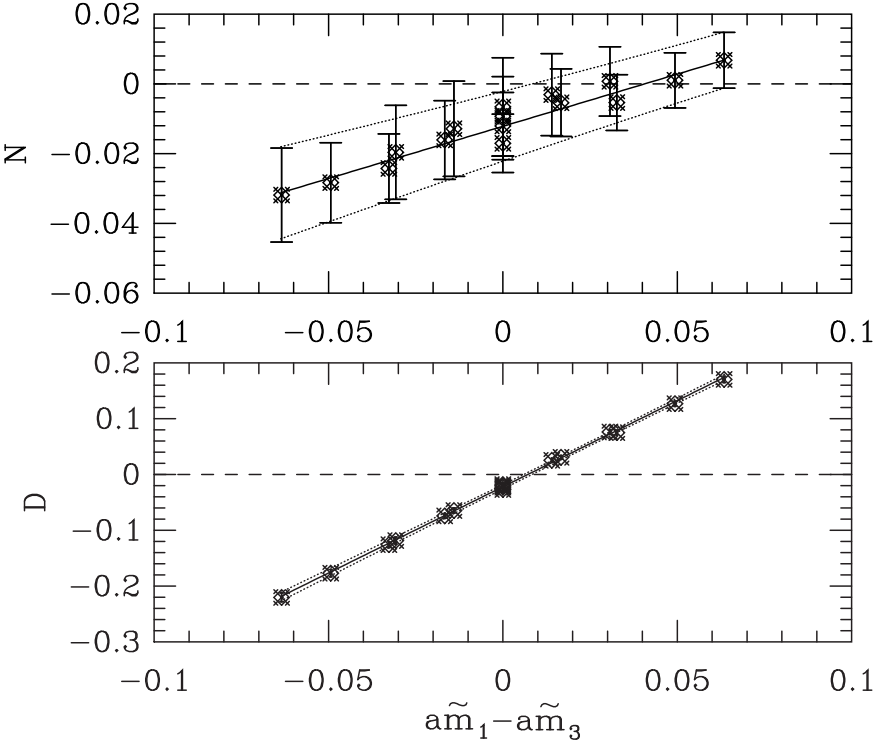


FIG. 11: **62NP** data for N and D used to extract c_V and defined in the text, plotted as a function of $\tilde{m}_1 - \tilde{m}_3$.

The ratio $B_\pi = M_\pi^2/\tilde{m}$ is much larger than Λ_{QCD} . Indeed, $B_\pi \approx 4 \text{ GeV}$ at our values of β , so that $aB_\pi/2 \approx 1$ at $\beta = 6$! Thus, although the r.h.s. of Eq. (24) is formally of $O(a^2)$, it can be comparable in magnitude to an $O(a)$ effect. Of course, the numerator also depends on c_A , although in a way which cannot be estimated simply. Thus, it is possible that the enhanced c_A dependence cancels in Z_V^0 , and our results indicate that this is what happens: 2- and 3-point discretizations lead to consistent results. This is an example of our general observation (see Sec. V) that the value of c_A determined from Eq. (15) improves the axial current in other correlation functions.

In contrast, the improvement of the axial current does not guarantee that there are no enhanced $O(a)$ errors in the slope, $\tilde{b}_V - \tilde{b}_A$ [8]. In particular, using a mass dependent c_A in $(A_I)_4^{(13)}$ produces an enhanced higher order effect proportional to B_π . We see this clearly in our results. For example, for the **62NP** data set, $\tilde{b}_V - \tilde{b}_A$ is $-0.11(3)$ [$-0.07(3)$] for the chirally extrapolated c_A and 2-point [3-point] discretization, while using the mass-dependent c_A these results change to $-0.30(4)$ [$+0.34(5)$]. It is reassuring that the discretization dependence is much weaker for chirally extrapolated c_A , since this is the choice we have made at the order of improvement that we are working (see Section II). These are the results we quote.

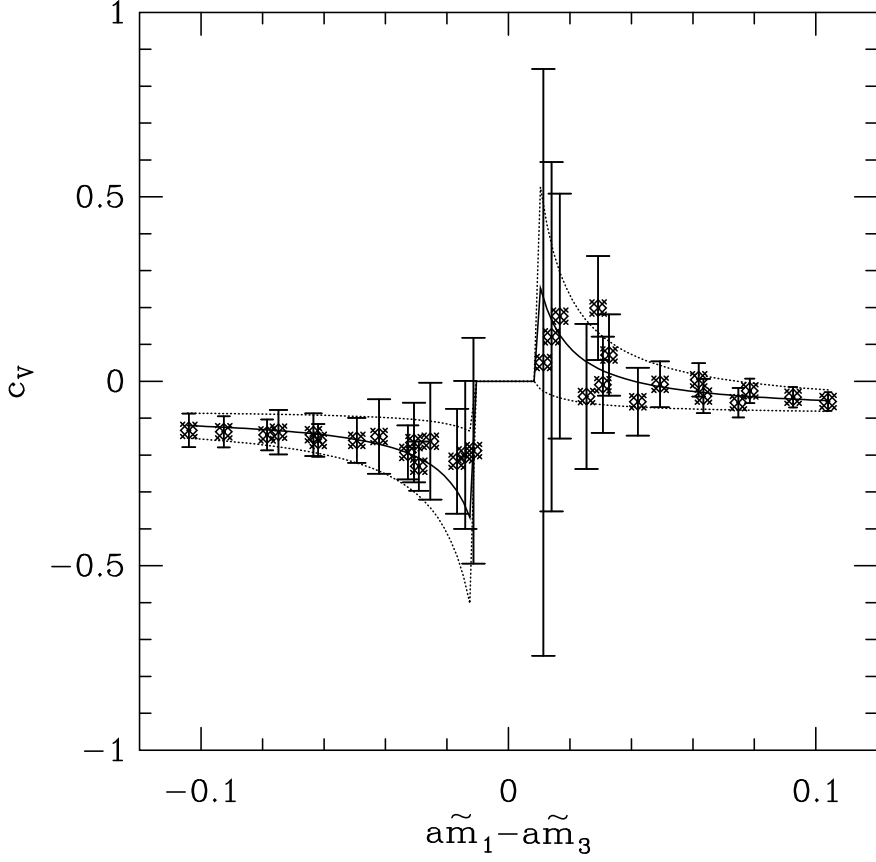


FIG. 12: A fit of the form $c_V = c_V^{(0)} + c_V^{(1)} / (\tilde{m}_1 - \tilde{m}_3)$ to the **62NP** data.

VIII. Z_A^0

The AWI which yields the best signal for Z_A^0 is

$$\frac{\sum_{\vec{y}} \langle \delta \mathcal{S}_I^{(12)} (A_I)_i^{(23)}(\vec{y}, y_4) V_i^{(31)}(0) \rangle}{\sum_{\vec{y}} \langle (V_I)_i^{(13)}(\vec{y}, y_4) V_i^{(31)}(0) \rangle} = \frac{Z_V^0 (1 + \tilde{b}_V a \tilde{m}_3 / 2)}{Z_A^0 \cdot Z_A^0 (1 + \tilde{b}_A a \tilde{m}_3 / 2)}, \quad (25)$$

which holds after extrapolation to $\tilde{m}_1 = \tilde{m}_2 = 0$. The intermediate state in these correlators is the vector meson. The quality of the signal for the ratio on the l.h.s. is illustrated in Fig. 15. An example of the fit versus $\tilde{m}_3/2$ is shown in Fig. 16. The resulting values for $Z_V^0/(Z_A^0)^2$ and $\tilde{b}_A - \tilde{b}_V$ are given in Tabs. III-VI. The latter have much larger errors than those in the determinations described in the previous section.

Rather than obtaining Z_A^0 by combining the results for $Z_V^0/(Z_A^0)^2$ with those obtained previously for Z_V^0 , it turns out to be better to use the product of the left hand sides of Eqs. (20) and (25), which yields $1/(Z_A^0)^2$ directly. Note that the linear \tilde{m}_3 dependence cancels in this product. The data, illustrated in Fig. 17, are consistent with this prediction. Our final results are obtained by a fitting a constant to the data, excluding the lightest two masses as they have poor signals, and also excluding the heaviest mass. Neither of these exclusions significantly affect the final result.

As shown in Tabs. III-VIII, the statistical errors in Z_A^0 are roughly an order of magnitude

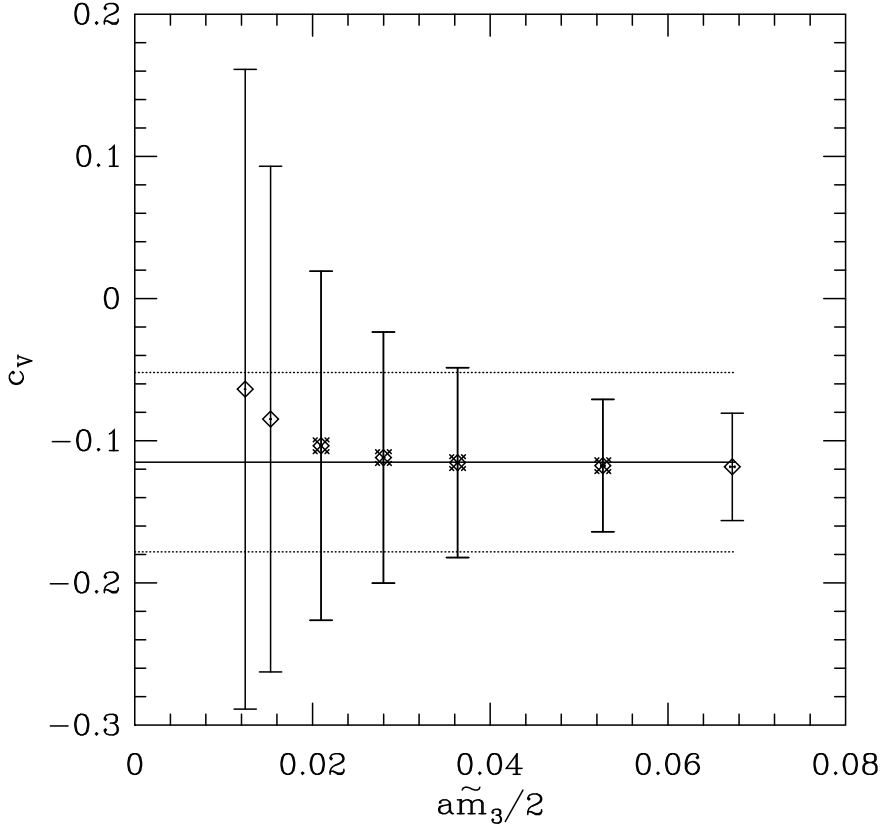


FIG. 13: A constant fit as a function of $\tilde{m}_3/2$ to extract c_V from the **62NP** data. Points included in the fit are superimposed with a fancy cross.

larger than those in Z_V^0 , and are comparable to the size of the expected $O(a^2)$ terms. Thus, either the statistical or the $O(a^2)$ corrections can explain the difference between our results and those of the ALPHA collaboration, which are at the $1 - 2\sigma$ level. The deviations from 1-loop perturbation theory are of the size expected if the 2-loop terms are $\sim \alpha_s^2$.

IX. Z_P^0/Z_S^0 , AND $\tilde{b}_S - \tilde{b}_P$

Our best estimates of $Z_P^0/(Z_S^0 Z_A^0)$ and $\tilde{b}_S - \tilde{b}_P$ are obtained from

$$\frac{\sum_{\vec{y}} \langle \delta \mathcal{S}_I^{(12)} S^{(23)}(\vec{y}, y_4) J^{(31)}(0) \rangle}{\sum_{\vec{y}} \langle P^{(13)}(\vec{y}, y_4) J^{(31)}(0) \rangle} = \frac{Z_P^0 (1 + \tilde{b}_P a \tilde{m}_3/2)}{Z_A^0 \cdot Z_S^0 (1 + \tilde{b}_S a \tilde{m}_3/2)}, \quad (26)$$

with $J = P$ or A_4 . Both numerator and denominator have pions as intermediate states, and have very good signals. Examples of their ratio are shown in Fig. 18. As discussed in Sec. V, this ratio should be independent of y_4 up to higher order discretization errors. These errors are expected to be larger for the **60TI** data set than for those with the non-perturbatively improved action, since the former are of $O(a)$, and the latter of $O(a^2)$. Our results are qualitatively consistent with these expectations, as illustrated in Fig. 18. Note that the scale is much finer for the lower graphs. A linear fit to Eq. (26) gives our estimates

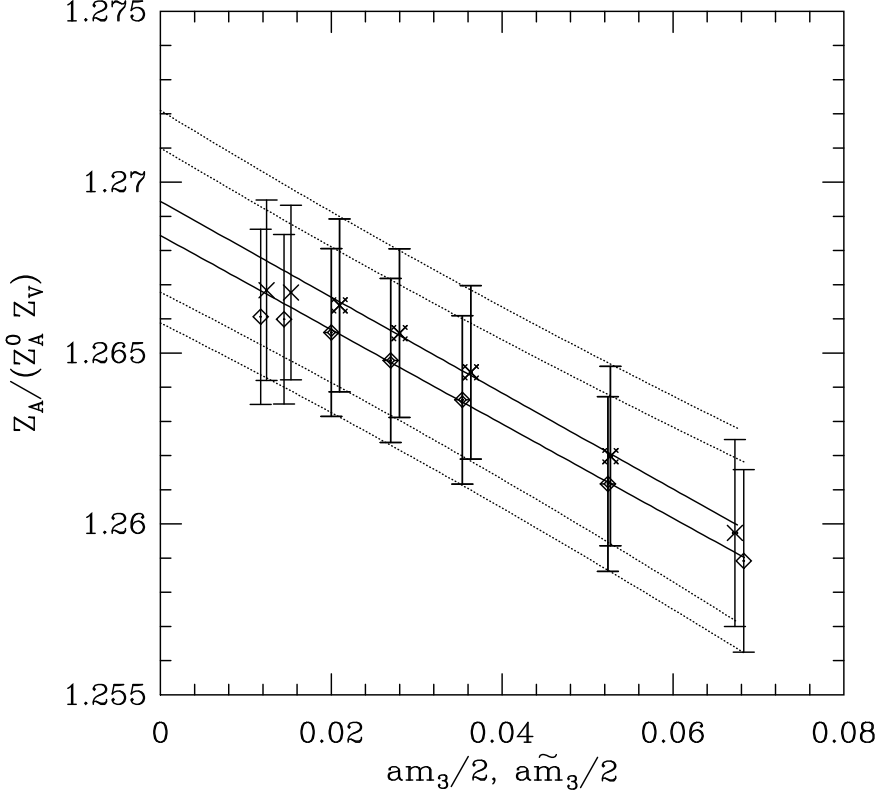


FIG. 14: Linear fits to the l.h.s. of Eq. (20) versus (i) the AWI quark mass \tilde{m} (crosses) and (ii) the VWI quark mass m (diamonds). The data set is **62NP**. The fit to crosses gives $\tilde{b}_A - \tilde{b}_V$, while that to diamonds gives $b_A - b_V$.

for $Z_P^0/(Z_S^0 Z_A^0)$ and $\tilde{b}_P - \tilde{b}_S$ quoted in the tables.

Another way to extract $Z_P^0/(Z_S^0 Z_A^0)$ is to use the relation between the two definitions of quark mass [11],

$$\frac{\tilde{m}}{m} = \frac{Z_P^0 Z_m^0}{Z_A^0} [1 - (\tilde{b}_A - \tilde{b}_P) a \tilde{m}_{av} + \tilde{b}_m a \frac{(\tilde{m}^2)_{av}}{\tilde{m}_{av}}], \quad (27)$$

where $X_{av} = (X_1 + X_2)/2$. This relation is useful because $Z_m^0 = 1/Z_S^0$ and $b_S = -2b_m$ [23, 24]. From the non-leading terms one can, using non-degenerate quarks, separately determine $\tilde{b}_A - \tilde{b}_P$ and \tilde{b}_m . In this section we discuss and use only degenerate quarks, from which one can determine $\tilde{b}_A - \tilde{b}_P - \tilde{b}_m$. The use of non-degenerate quarks, which allows a separate determination of $\tilde{b}_A - \tilde{b}_P$ and \tilde{b}_m , is discussed in Sec. XI.

We have analyzed Eq. (27) by extracting \tilde{m} from Eq. (15) using both the mass dependent and chirally extrapolated values of c_A . An example of the data and linear fits is shown in Fig. 19. The intercepts are consistent, and we quote, in Tabs. III-VI, the results using the mass-dependent c_A . We also show in the same figure the fit to Eq. (26), which should have the same intercept up to $O(a^2)$ terms. While the data show no significant discrepancy, the results from Eq. (27) can have enhanced discretization errors. Indeed, it follows from

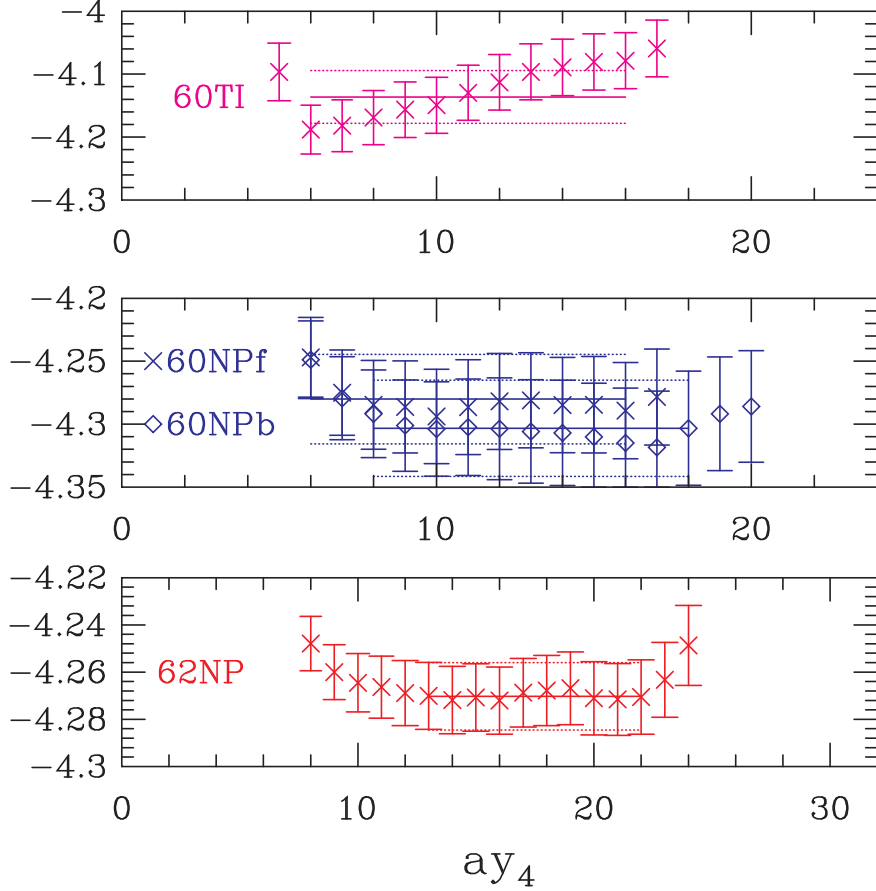


FIG. 15: Illustration of the signal for the ratio defined in Eq. (25) for the four data sets, using κ_3 propagators in all cases.

Eq. (15) that a change Δc_A results in

$$\frac{\Delta \tilde{m}}{\tilde{m}} = \Delta c_A a \frac{M_\pi^2}{2\tilde{m}} = \Delta c_A a B_\pi. \quad (28)$$

This is also the fractional change in the result for $Z_P^0/(Z_S^0 Z_A^0)$ obtained from Eq. (27). Since, as noted above, $B_\pi \sim 4$ GeV, this nominally $O(a^2)$ uncertainty can be enhanced. As a result, we consider the evaluation using Eq. (27) less reliable than that based on Eq. (26), and we use the latter as our best estimate.

The slope of the linear fits to Eq. (27) for degenerate quarks gives $\tilde{b}_A - \tilde{b}_P + \tilde{b}_S/2$. The statistical errors on the results are small, but there is a systematic dependence on whether we use the mass-dependent or chirally extrapolated c_A —an $O(a)$ effect enhanced by B_π . This problem is clear from Fig. 19, and to highlight the magnitude we quote both values in Tabs. III–VI: the first corresponds to the mass-dependent c_A and the second to the chirally extrapolated c_A . Unlike the case of $\tilde{b}_A - \tilde{b}_V$, here the mass-independent c_A , which is our choice, leads to results which depend very strongly on the choice of discretization. Because of these very large $O(a^2)$ effects, we do not use these estimates any further.

Our derived results for Z_P^0/Z_S^0 , presented in Tab. VIII, are significantly smaller than the predictions of 1-loop perturbation theory. As noted in Sec. IV, the difference can only be

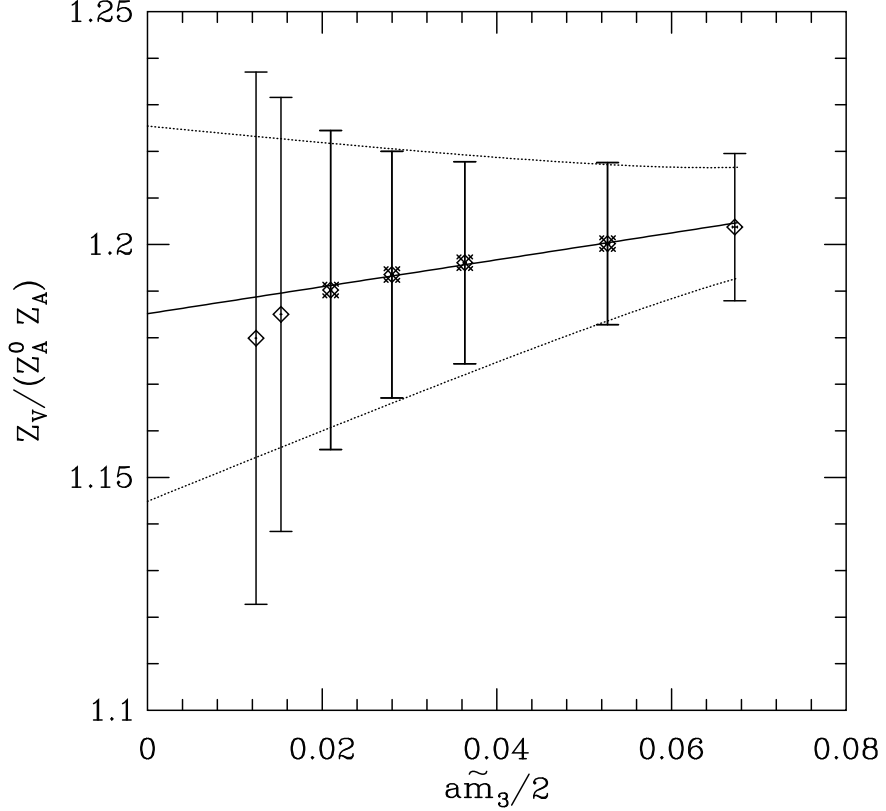


FIG. 16: Linear fit to the ratio defined in Eq. (25) after extrapolation to $\tilde{m}_1 = \tilde{m}_2 = 0$ for the **62NP** data set.

explained by an unlikely 2-loop contribution $\sim 4\alpha_s^2$.

X. c_T

To determine c_T we consider the AWI for the bilinear T_{ij} , *i.e.*

$$Z_A^0 \frac{\sum_{\vec{y}} \langle \delta \mathcal{S}_I^{(12)} (T_I)_{ij}^{(23)}(\vec{y}, y_4) T_{k4}^{(31)}(0) \rangle}{\sum_{\vec{y}} \langle (T_I)_{k4}^{(13)}(\vec{y}, y_4) T_{k4}^{(31)}(0) \rangle} = 1 \quad (29)$$

As was the case for c_V , tuning c_T in order to make the ratio independent of y_4 does not work. Instead we rewrite the identity in the following form,

$$1 + ac_T \frac{\sum_{\vec{y}} \langle [-\partial_4 V_k]^{(13)}(\vec{y}, y_4) T_{k4}^{(31)}(0) \rangle}{\sum_{\vec{y}} \langle T_{k4}^{(13)}(\vec{y}, y_4) T_{k4}^{(31)}(0) \rangle} = Z_A^0 \frac{\sum_{\vec{y}} \langle \delta \mathcal{S}_I^{(12)} T_{ij}^{(23)}(\vec{y}, y_4) T_{k4}^{(31)}(0) \rangle}{\sum_{\vec{y}} \langle T_{k4}^{(13)}(\vec{y}, y_4) T_{k4}^{(31)}(0) \rangle}, \quad (30)$$

where we have moved the c_T dependence in $(T_I)_{k4}$ onto the l.h.s., and used the fact that $(T_I)_{ij}$ has no contribution from the c_T term at $\vec{p} = 0$. Given Z_A^0 , Eq. (30) determines c_T after the $m_1 \rightarrow 0$ extrapolation. The data for the ratios on the left and right hand sides of Eq. (30) are illustrated in Figs. 20 and 21 respectively and expose the reason for the

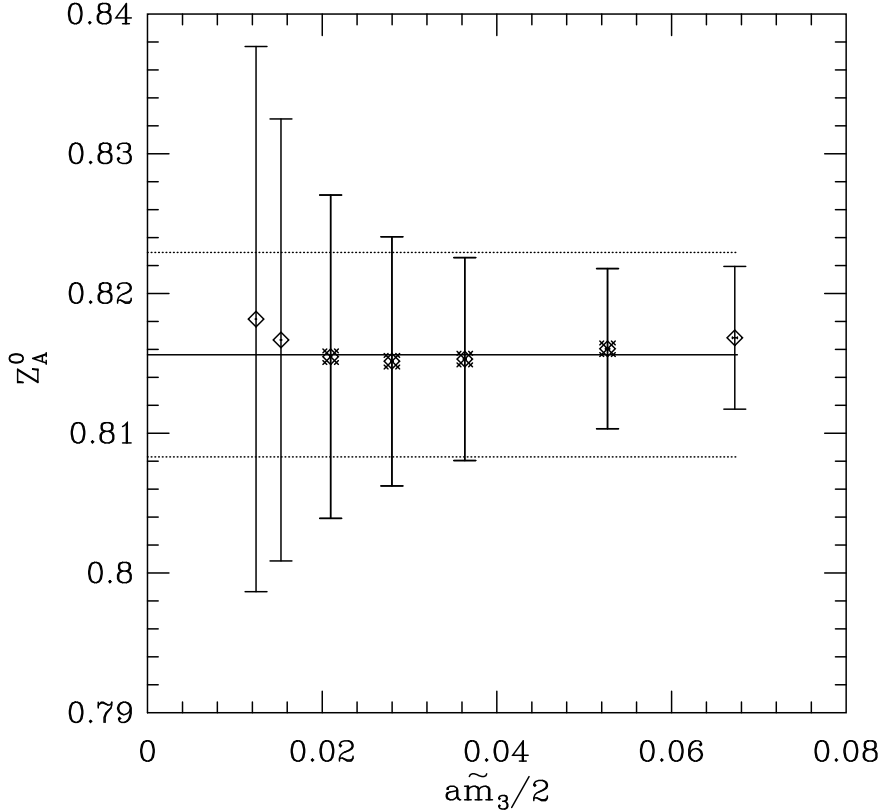


FIG. 17: Z_A^0 , obtained from the product of ratios of correlators defined in the l.h.s. of Eq. (20) and Eq. (25), shown as a function of $\tilde{m}_3/2$. The constant fit is to the $\kappa_2 - \kappa_5$ points, as indicated by the fancy crosses. The data set is **62NP**.

failure to extract c_T by tuning with respect to y_4 : the two ratios are essentially flat within the domain of the chiral rotation (which roughly corresponds to the region of the fits in the Figure).

c_T should be independent of \tilde{m}_3 , up to corrections of $O(a^2)$. Our results are consistent with this expectation, as illustrated in Fig. 22 for the **62NP** data set. Our quoted results are the weighted average over the $\kappa_2 - \kappa_5$ points.

To extract b_T using the method proposed in [8] requires studying this AWI with all three quarks in Eq. (30) having different masses. We have not done this extended calculation, and consequently have no results for b_T .

XI. ADDITIONAL RELATIONS

There are two additional relations that can be used to obtain information on improvement constants. These were derived in Ref. 11, and discussed further in Ref. 8. The first is

$$\tilde{b}_P - \tilde{b}_A = -\frac{4\tilde{m}_{12} - 2[\tilde{m}_{11} + \tilde{m}_{22}]}{a[\tilde{m}_{11} - \tilde{m}_{22}]^2}. \quad (31)$$

An illustration of our results for the r.h.s. is shown in Fig. 23, and the results from fits to a constant are collected in Tabs. III-VI, and used to obtain the final results given in Tab. VIII.

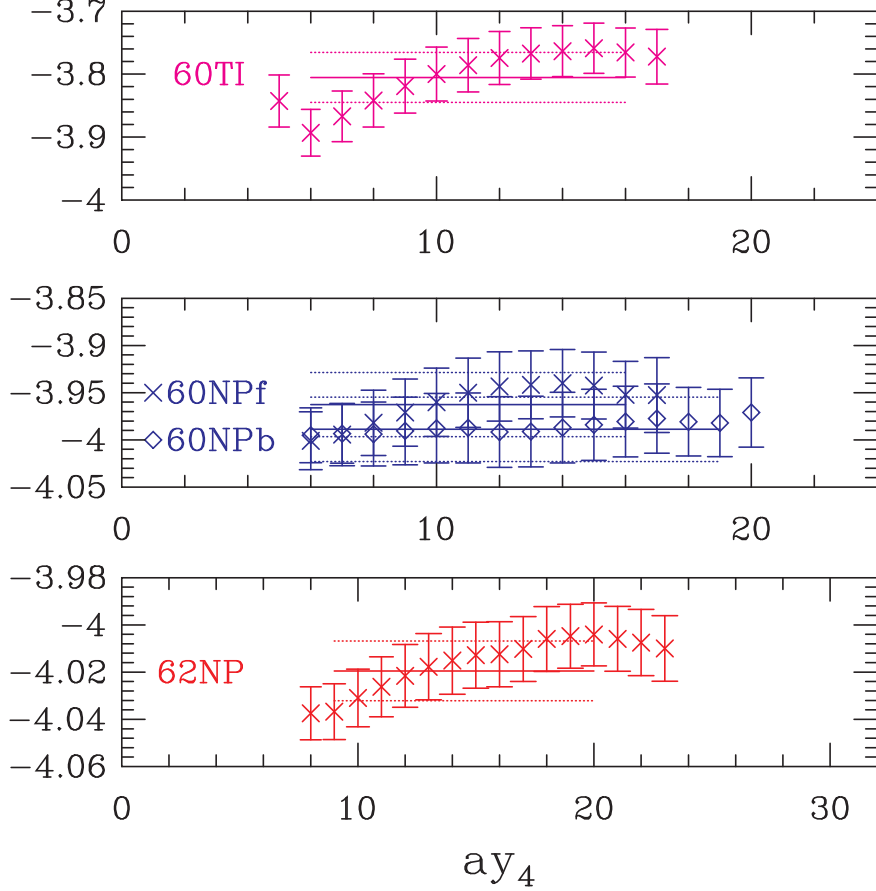


FIG. 18: Comparison of the signal in the ratio of correlators on the l.h.s. of Eq. (26) used to extract Z_P^0/Z_S^0 . The data are for κ_3 propagators in all cases.

The second relation is

$$\frac{\tilde{b}_S - \tilde{b}_V}{2} + (\tilde{b}_P - \tilde{b}_A) = \frac{\Delta_{12} - R_Z[\tilde{m}_{11} - \tilde{m}_{22}]}{aR_Z[\tilde{m}_{11}^2 - \tilde{m}_{22}^2]}, \quad (32)$$

$$\Delta_{12} \equiv \frac{\sum_{\vec{x}} e^{i\vec{p}\cdot\vec{x}} \langle \partial_\mu V_{I\mu}^{(12)}(\vec{x}, t) J^{(21)}(0) \rangle}{\sum_{\vec{x}} e^{i\vec{p}\cdot\vec{x}} \langle S^{(12)}(\vec{x}, t) J^{(21)}(0) \rangle} \quad (33)$$

$$R_Z \equiv \frac{Z_S^0}{Z_P^0} \cdot \frac{Z_A^0}{Z_V^0}. \quad (34)$$

As discussed in Ref. 8, of the two kinds of sources: $J^{(21)} = \sum_{\vec{z}} P^{(23)}(\vec{z}, z_4) P^{(31)}(0)$, and $J^{(21)} = S^{(21)}$ with $0 < t < z_4$ that one can use in Eq. (33), the first has a better signal and smaller discretization errors. Unfortunately, the final results, quoted in the Tables, have very large errors due to large cancellations between the terms in the numerator on the r.h.s.. We, therefore, do not use this second combination in our final extraction of the individual \tilde{b} 's given in Tab. VIII.

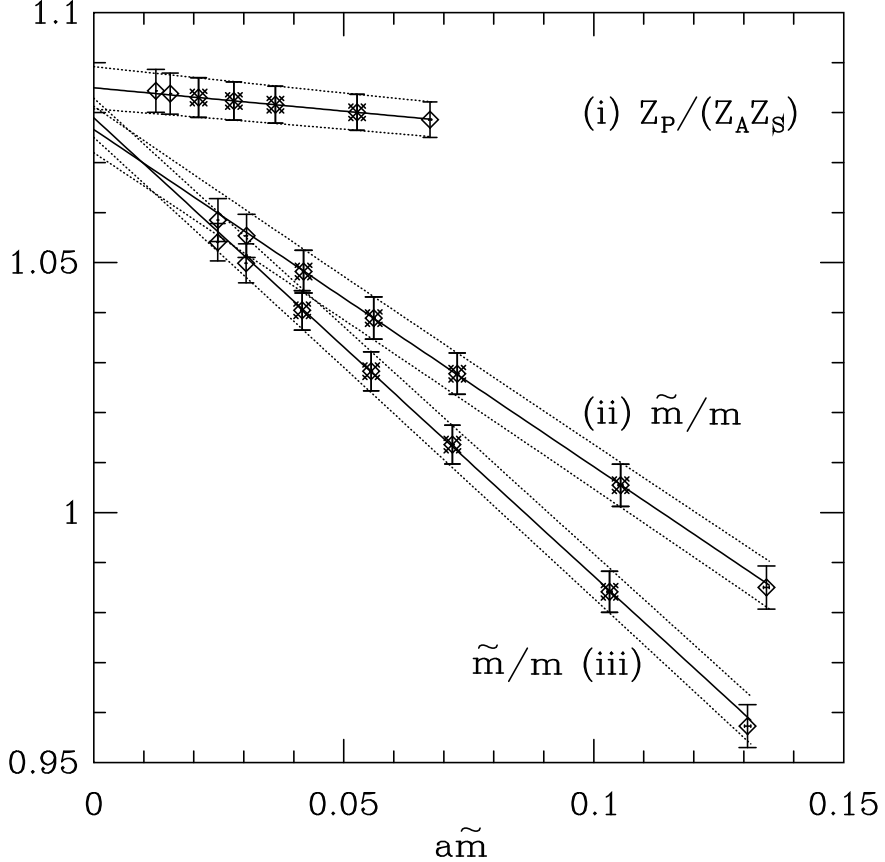


FIG. 19: Comparison of the quality of the linear fits used to extract $Z_A^0 Z_S^0 / Z_P^0$. The three fits correspond to (i) Eq. (26), (ii) Eq. (27) with \tilde{m} defined using the mass dependent c_A , and (iii) Eq. (27) with \tilde{m} defined using the chirally extrapolated c_A . The data are from the **62NP** set. Note that the intercepts from all three fits should agree up to errors of $O(a^2)$, but the slope of (i) is $b_P - b_S$ whereas those of (ii) and (iii) are $b_P - b_A - b_S/2$.

XII. EQUATION-OF-MOTION OPERATORS

The method for calculating the combination $c'_P + c'_{\mathcal{O}}$ of coefficients of equation-of-motion operators has been described in Sec. II. The calculation, using Eq. (14), involves three pieces. The slopes $s_{\mathcal{O}}$ are obtained from a linear fit to the l.h.s. of Eq. (10) versus \tilde{m}_1 at fixed \tilde{m}_3 . Examples of these fits are shown in Fig. 24, for the **62NP** data set. The on-shell quantities $X_{\mathcal{O}}(\tilde{b}_{\delta\mathcal{O}} - \tilde{b}_{\mathcal{O}})$ and $X_{\mathcal{O}}\tilde{b}_A$ can be obtained by combining results discussed in previous sections. The results for these three contributions, for the **62NP** data set, are collected in Tab. X. We find that $X_{\mathcal{O}}\tilde{b}_A$ gives almost the entire contribution. The final estimates for individual equation-of-motion constants are given in Tab. IX.

We briefly discuss some details of the calculation, and the quality of the signal, in each of the five cases.

- $c'_P + c'_{\mathcal{V}}$: We choose $J = P$ and $\mathcal{O} = V_4$ ($\delta\mathcal{O} = A_4$), in which case the intermediate state is a pseudoscalar.
- $c'_P + c'_A$: We choose $J = V_i$ and $\mathcal{O} = A_i$ ($\delta\mathcal{O} = V_i$) whereby the intermediate state is

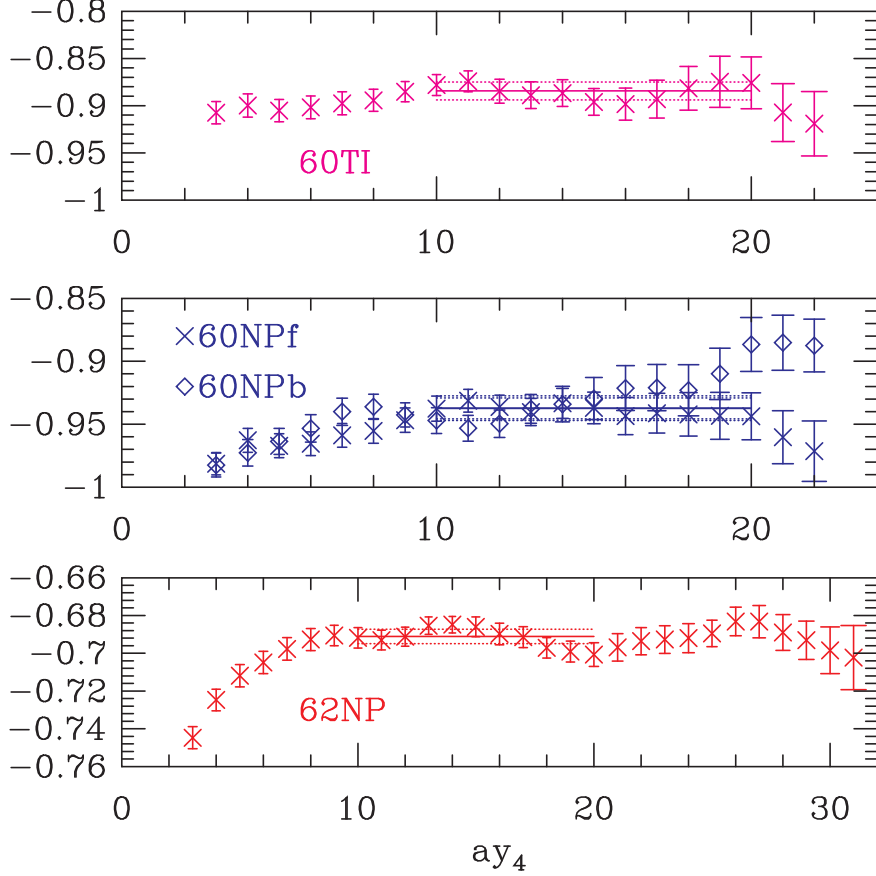


FIG. 20: The signal in the ratio of correlators defined on the left hand side of Eq. (30) using κ_3 in all quark propagators.

a vector meson. Unfortunately, the uncertainty in c_V feeds in through $\delta\mathcal{O} = V_i$ and affects the extraction of s_A . Thus, even though s_A contributes little to the central value of $c'_P + c'_A$, as illustrated in Tab. X, it dominates the error.

- $2c'_P$: We choose $J = S$ and $\mathcal{O} = P$ ($\delta\mathcal{O} = S$). In this case, the intermediate state is a scalar and the signal is poor.⁵ The largest part of the error in c'_P comes from s_P . The resulting uncertainty in c'_P dominates the error in the final estimate of c'_V , c'_S , and c'_T .
- $c'_P + c'_S$: The choice $J = P$ and $\mathcal{O} = S$ ($\delta\mathcal{O} = P$) gives a good signal in the correlation functions as the intermediate state is pseudoscalar.
- $c'_P + c'_T$: We choose $J = T_{k4}$ and $\mathcal{O} = T_{ij}$ ($\delta\mathcal{O} = T_{k4}$). All correlation functions have a good signal as the intermediate state is a vector meson.

The signal for s_V , s_S , and s_T is good for all \tilde{m}_3 , and leads to a reliable estimates with comparable errors for $c'_P + c'_V$, $c'_P + c'_S$, and $c'_P + c'_T$. In all cases we find that $s_{\mathcal{O}}$ are

⁵ A better choice might be to use $J = \sum_z P(z)P(0)$ with $z_4 \gg y_4 \gg 0$, in which case the intermediate state is pseudoscalar, but this requires an extra inversion.

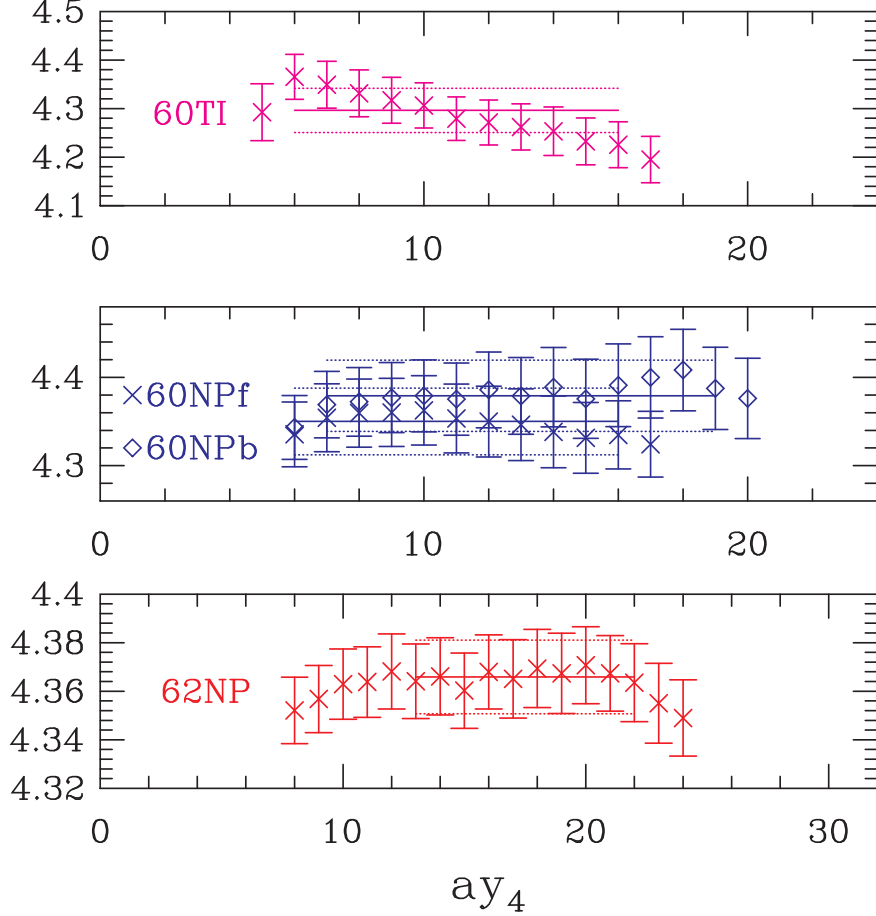


FIG. 21: The signal in the ratio of correlators defined on the right hand side of Eq. (30) using κ_3 in all quark propagators.

$c'_O + c'_P$	s_O	$X_O(b_{\delta O} - b_O)/2$	$X_O b_A$
$c'_V + c'_P$	-0.27(04)	-0.07(2)	1.52(4)
$c'_A + c'_P$	-0.13(06)	0.07(2)	1.41(3)
$c'_P + c'_P$	-0.73(16)	0.06(2)	1.70(7)
$c'_S + c'_P$	-0.14(03)	-0.05(1)	1.29(3)
$c'_T + c'_P$	-0.23(05)	0.02(3)	1.46(4)

TABLE X: The three contributions to the coefficient of the equation of motion operators $c'_O + c'_P$ for the **62NP** data set.

independent of \tilde{m}_3 within statistical errors. Our final results are given by the weighted mean over \tilde{m}_3 corresponding to $\kappa_2 - \kappa_5$.

To compare to the predictions of perturbation theory, it is best to use the results for $c'_X + c'_P$, $X = V, A, S, T$, in the upper part of Table IX, since these have the smallest statistical errors. These four quantities are indeed consistent with the expected result $2[1 + O(\alpha_s) + O(a)]$. The fifth quantity, $2c'_P$, is only determined reliably at $\beta = 6.2$, and also

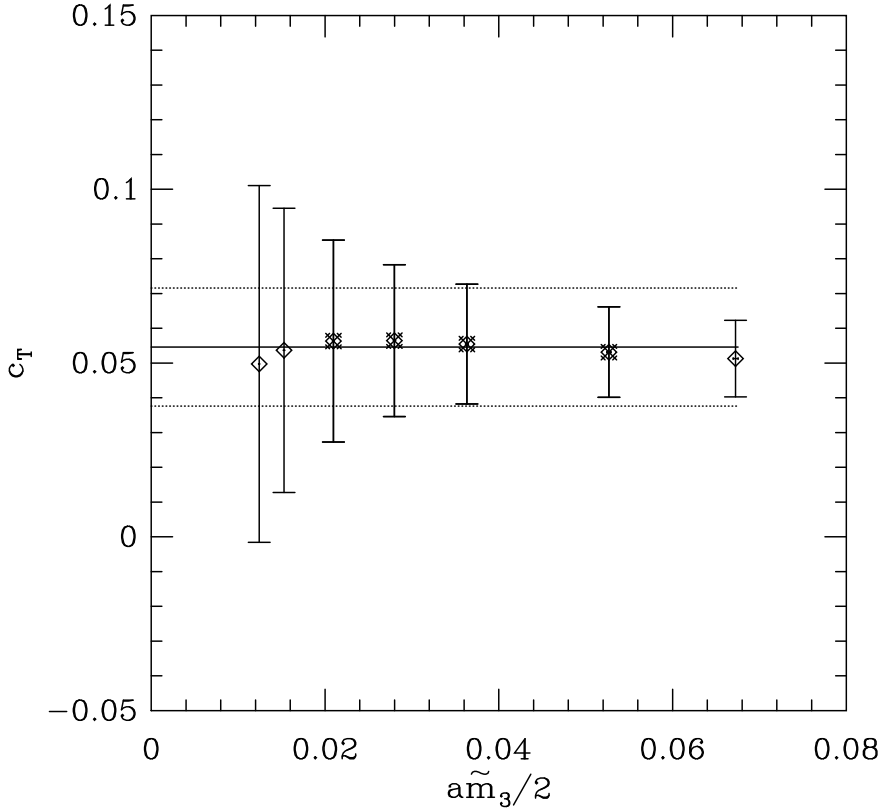


FIG. 22: Estimates of c_T as a function of $\tilde{m}_3/2$ for the **62NP** data set. The constant fit is to the $\kappa_2 - \kappa_5$ points.

agrees with this expectation. These agreements are a consistency check on the extension of the improvement program to off-shell quantities.

XIII. CONCLUSION

We have demonstrated the feasibility of the WI method, with non-degenerate quark masses, for determining the improvement and scheme-independent normalization constants of the quark bilinear operators. The main advantage of using non-degenerate quarks is that one can extract all the \tilde{b}_X . These quantities effect the overall normalization of operators away from the chiral limit, and their determination is relevant to phenomenological applications involving heavy mesons.

Our implementation of the Ward identities differs substantially from that used by the ALPHA collaboration, so that the results from the two methods can differ. These differences, should, however, be of size $O(a)$ and $O(a^2)$, respectively, for improvement and normalization constants. The differences between the two sets of results are, in fact, consistent with these expectations. We stress, however, that for the small quantities, c_A and c_V , this “consistency” allows a substantial uncertainty at $\beta = 6$. For example, $\Delta c_A = 0.05$ would lead to an $\approx 10\%$ uncertainty in f_π and 3% in f_D . At $\beta = 6.2$, on the other hand, there is a much smaller variability.

Both c_V and c_T are obtained as a small difference between two large terms. We are,

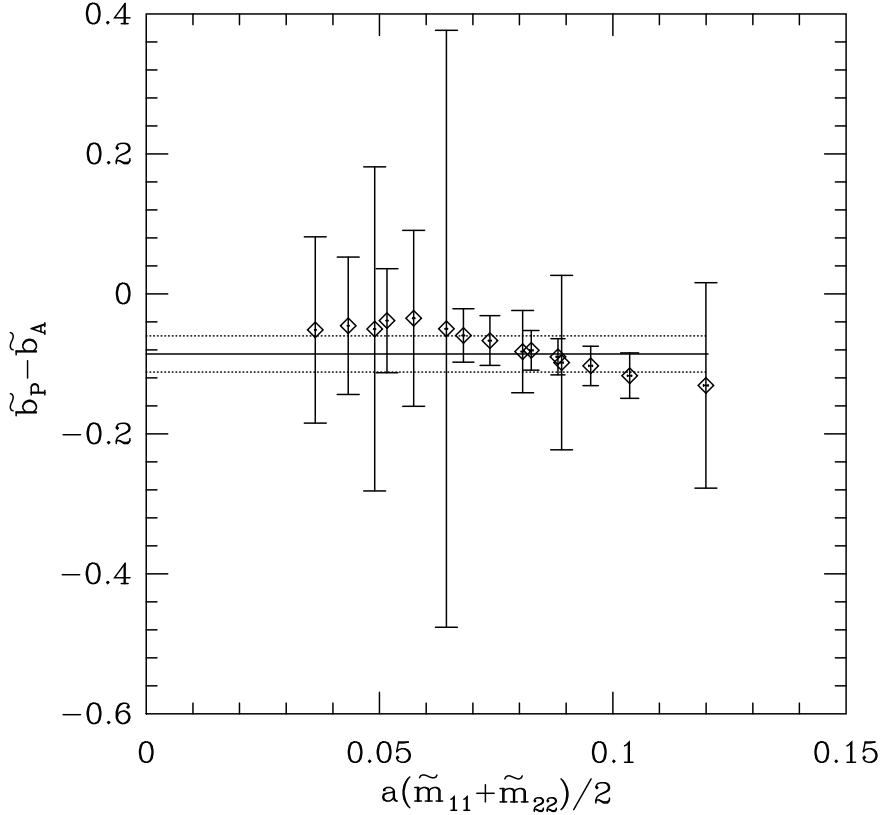


FIG. 23: A constant fit to the **62NP** data for $\tilde{b}_P - \tilde{b}_A$ obtained using Eq. (31).

nevertheless, able to extract these quantities with reasonable precision. In particular, in the case of c_V , we find that our best results come from enforcing a different Ward identity than considered previously, with a consequent reduction in errors. This improvement is important for phenomenological applications (see, *e.g.*, Ref. 25), and also leads to smaller errors in our results for Z_A^0 , Z_P^0/Z_S^0 , c_T and c'_A .

On the whole, tadpole-improved 1-loop perturbation theory underestimates the deviations of renormalization and improvement constants from their tree level values. In all but one case, however, these discrepancies can be understood as a combination of a 2-loop correction of size $(1-2) \times \alpha_s^2$ [for Z_V^0 , Z_A^0 , and c_A], higher order discretization errors of size $(1-2) \times a\Lambda_{\text{QCD}}$ [for c_V , c_T and \tilde{b}_V], and statistical errors [for \tilde{b}_A , \tilde{b}_P , and \tilde{b}_S]. The only exception is Z_P^0/Z_S^0 , for which a very large higher order perturbative contribution of size $4 \times \alpha_s^2$ is needed to reconcile our non-perturbative results with 1-loop perturbation theory.

We have, for the first time, presented results for the coefficients of equation of motion operators that are needed to improve the theory off-shell. The most striking feature of their calculation is the improvement in the reliability of the calculation between $\beta = 6.0$ and 6.2 .

An important issue is at what quark mass $O(a)$ improvement breaks down, due to our neglect of higher order terms. To address this issue we examine the case of the charm quark at $\beta = 6.2$ for which $ma \approx 0.5$ and $\tilde{m} \approx 0.4$. Since $\tilde{b}_X \approx 1.1$, the $O(a)$ corrections to Z_X^0 are approximately 45%. Assuming geometric growth, this would imply $\approx 20\%$ correction from the neglected $O(a^2)$ terms. This is indeed what we find for Z_V , for which non-perturbative results for charm quarks are available, and the data are good enough to allow the quadratic

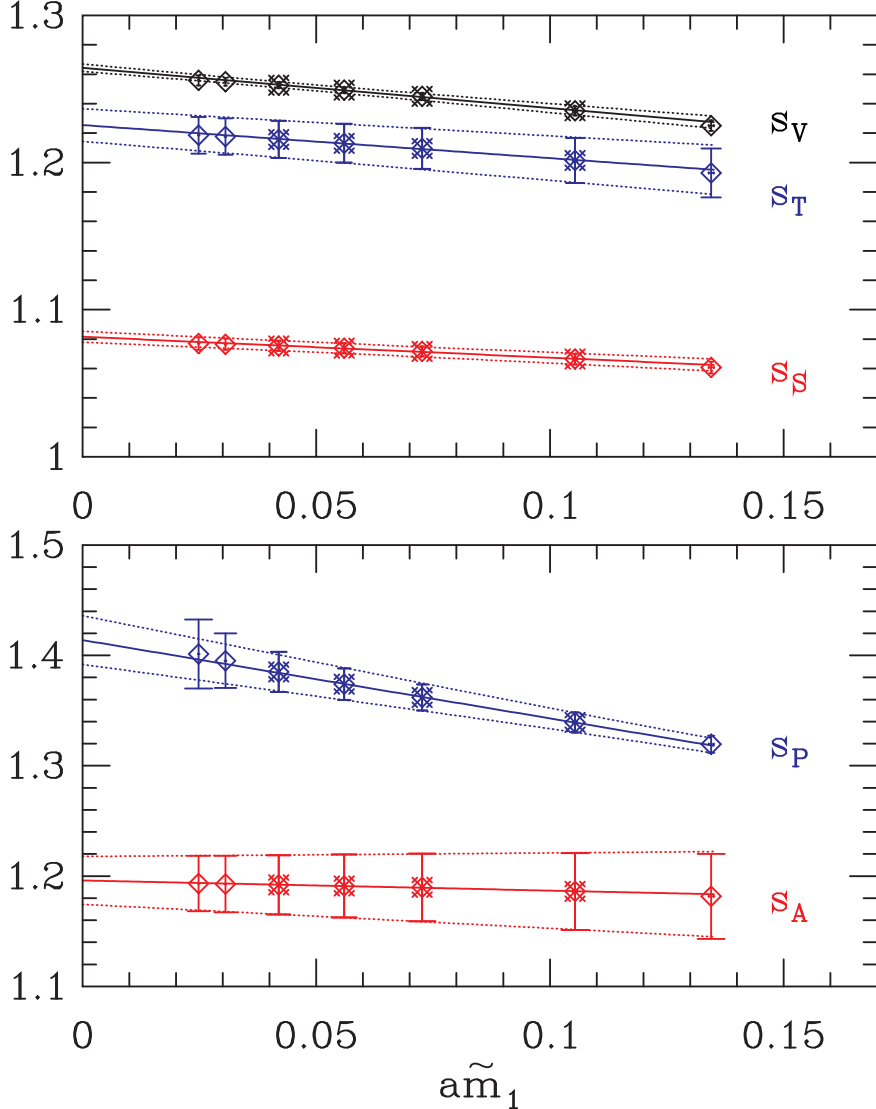


FIG. 24: Linear fits to the l.h.s. of Eq. (10), the slopes of which, $s_{\mathcal{O}}$, determine the coefficients of the equation of motion operators. The data set is **62NP** and \tilde{m}_3 corresponds to κ_3 .

fit given in Eq. (18). On the other hand, we find that if we use the alternative $O(a)$ improved expression $Z_V = Z_V^0(1 + b_V m a)$, it works to within 1% at the charm quark mass.

Finally, we stress that the use of non-degenerate quarks to determine the \tilde{b}_X and c_T could be applied equally well in the context of the Schrödinger functional. It would be very interesting to compare results so obtained to those we have found here.

Acknowledgments

These calculations were done at the Advanced Computing Laboratory at Los Alamos and at the National Energy Research Scientific Computing Center (NERSC) under a DOE Grand Challenges grant. The work of T.B., R.G., and W.L. was, in part, supported by DOE

grant KA-04-01010-E161 and of S.R.S by DE-FG03-96ER40956/A006.

APPENDIX A

In this appendix we review the relation between continuum and lattice fields and the 1-loop perturbative results. Throughout this paper we use

$$(\mathcal{O}_R)_{\text{continuum}}^{(ij)} = \sqrt{4\kappa_i\kappa_j}(\mathcal{O}_R)_{\text{lattice}}^{(ij)}. \quad (\text{A1})$$

This normalization makes comparison between tadpole-improved 1-loop and non-perturbative results, quoted in Tab. VIII, straightforward. In the tadpole improved theory [26], the normalization commonly used is $\sqrt{4\kappa_i\kappa_j}u_0^2$. To maintain the field normalization as $\sqrt{4\kappa_i\kappa_j}$ we have absorbed u_0 into $Z_{\mathcal{O},\text{pert}}^0$. Consequently, the TI perturbative result we use is $Z_{\mathcal{O},\text{pert}}^0 = u_0(1 + t_{\mathcal{O}}\alpha_S^{TI})$, where $t_{\mathcal{O}}$ is the TI 1-loop coefficient.

A second way in which tadpole improvement is defined is

$$\begin{aligned} (\mathcal{O}_R)_{\text{continuum}}^{(ij)} &= 8\kappa_c \sqrt{1 - \frac{3\kappa_i}{4\kappa_c}} \sqrt{1 - \frac{3\kappa_j}{4\kappa_c}} Z_{\mathcal{O},\text{pert}}^0(\mathcal{O})_{\text{lattice}}^{(ij)} \\ &= \sqrt{4\kappa_i\kappa_j} \sqrt{1 + 8\kappa_c(\frac{1}{2\kappa_i} - \frac{1}{2\kappa_c})} \sqrt{1 + 8\kappa_c(\frac{1}{2\kappa_j} - \frac{1}{2\kappa_c})} Z_{\mathcal{O},\text{pert}}^0(\mathcal{O})_{\text{lattice}}^{(ij)} \end{aligned} \quad (\text{A2})$$

where we have again absorbed a factor of u_0 in $Z_{\mathcal{O},\text{pert}}^0$ to maintain the same definition as above. Eq. (A2) shows that using tadpole-improved field renormalization is equivalent, at $O(a)$, to using $b_{\mathcal{O}} = 8\kappa_c$ in Eq. (3). In tree-level TI perturbation theory $8\kappa_c = 1/u_0$, and is the appropriate value for $b_{\mathcal{O}}$ as shown in Eq. (A6).

The 1-loop perturbative calculations have been done by the ALPHA and JLQCD collaborations [27, 28, 29]. Here we express the results for the tadpole improvement scheme stated above. Tadpole improvement requires choosing a quantity, u_0 , which is unity at tree-level, whose perturbative series is dominated by a tadpole contribution, and which can be evaluated non-perturbatively. Any other quantity X , whose perturbative expansion is

$$X = X^{(0)} + X^{(1)}\alpha_s, \quad (\text{A3})$$

and which is dominated by n contributions of the tadpole diagram, can then be re-written as

$$X_{TI} = u_0^n(X^{(0)} + X_{TI}^{(1)}\alpha_{s,TI}),$$

where

$$X_{TI}^{(1)} = X^{(1)} - nX^{(0)}u_0^{(1)}. \quad (\text{A4})$$

Here $u_0^{(1)}$ is the coefficient of α_s in the perturbative expansion of u_0 , and $\alpha_{s,TI}$ is an improved coupling that we choose to be $g^2/4\pi u_0^4$, where $\beta = 6/g^2$. Since all results we quote are tadpole-improved, we henceforth omit the subscript TI for brevity.

In this paper, we choose, for u_0 , the fourth root of the expectation value of the plaquette for which $u_0^{(1)} = -\pi/3$. Our Monte Carlo data yields $u_0 = 0.8778$ at $\beta = 6.0$ and 0.8851 at $\beta = 6.2$. Using this u_0 , we find that $\alpha_s = 0.1340$ and 0.1255 at the two β 's.

Γ	γ_Γ	$z_\Gamma^{(1)}$	$c_\Gamma^{(1)}$	$b_\Gamma^{(1)}$	$\tilde{b}_\Gamma^{(1)}$
S	1	-1.002		1.3722	1.2818
P	1	-1.328		0.8763	0.7859
V	0	-0.579	-0.2054	0.8796	0.7892
A	0	-0.416	-0.0952	0.8646	0.7742
T	-4/3	-0.134	-0.1505	0.7020	0.6116

TABLE XI: The tadpole-improved one-loop coefficients in Eq. (A6). The tadpole-improvement factor, u_0 , has been chosen to be the fourth root of the plaquette expectation value.

At one-loop, the coefficient of the clover term is

$$c_{SW} = u_0^{-3} (1 + c_{SW}^{(1)} \alpha_s), \quad (\text{A5})$$

where $c_{SW}^{(1)} = 0.214$ is obtained by converting the results by Wohlert [30] and the ALPHA collaboration [31] to tadpole-improved form. Then $c_{SW} = 1.521$ and 1.481 at $\beta = 6.0$ and 6.2 respectively.

The tadpole-improved renormalization constants at one loop are given by the formulæ:

$$\begin{aligned} Z_\Gamma^0 &= u_0 [1 + \alpha_s (\frac{\gamma_\Gamma}{4\pi} \ln(\mu a)^2 + z_\Gamma^{(1)})] \\ c_\Gamma &= \alpha_s c_\Gamma^{(1)} \\ b_\Gamma &= u_0^{-1} [1 + \alpha_s b_\Gamma^{(1)}] \\ \tilde{b}_\Gamma &= [1 + \alpha_s \tilde{b}_\Gamma^{(1)}] \end{aligned} \quad (\text{A6})$$

where μ is the scale at which the continuum $\overline{\text{MS}}$ theory is defined. The final results for all these tadpole-improved coefficients are given in Tab. XI. There are two points worth noting: (i) the tadpole factors cancel in the product $b_\Gamma m$, whereas neither \tilde{b}_Γ nor \tilde{m} has any; (ii) the one-loop correction, $c_{SW}^{(1)}$, does not contribute to the renormalization or improvement constants at $O(\alpha_s)$.

APPENDIX B

In this appendix we review tree-level improvement of Wilson fermions and define our conventions for improvement coefficients. The $O(a)$ improvement of Wilson fermions can be obtained by the transformation [32],

$$\begin{aligned} \psi \rightarrow \psi_I &= \left[1 - \frac{ar}{4} (\vec{\mathcal{D}} - m) \right] \psi \\ \bar{\psi} \rightarrow \bar{\psi}_I &= \bar{\psi} \left[1 + \frac{ar}{4} (\vec{\mathcal{D}} + m) \right], \end{aligned} \quad (\text{B1})$$

where the continuum equation of motion is given by $(\overrightarrow{\mathcal{D}} + m)\psi = 0$. Using the fact that the Wilson-clover operator $a\mathcal{W}$ is related to $\overrightarrow{\mathcal{D}}$ by

$$\begin{aligned} a\overrightarrow{\mathcal{W}}\psi &= a(\overrightarrow{\mathcal{D}} + m)\psi + O(a^2) \\ \overleftarrow{\psi}a\overleftarrow{\mathcal{W}} &= \overleftarrow{\psi}(\overleftarrow{\mathcal{D}} - m)a + O(a^2), \end{aligned} \quad (B2)$$

we can rewrite the improved fermion fields ψ_I and $\overline{\psi}_I$ as

$$\begin{aligned} \psi_I &= \left\{ 1 - \frac{ar}{4} [c_{swr}\overrightarrow{\mathcal{D}} - (2 - c_{swr})m] - \frac{ar(1 - c_{swr})}{4}\overrightarrow{\mathcal{W}} \right\} \psi + O(a^2) \\ \overline{\psi}_I &= \overline{\psi} \left\{ 1 + \frac{ar}{4} [c_{swr}\overleftarrow{\mathcal{D}} + (2 - c_{swr})m] + \frac{ar(1 - c_{swr})}{4}\overleftarrow{\mathcal{W}} \right\} + O(a^2), \end{aligned} \quad (B3)$$

where c_{swr} represents an arbitrary ‘rotation’ parameter. Operators composed of these improved fermion fields are automatically $O(a)$ improved at tree level.

In particular, we can construct the tree-level improved fermion bilinears S , P , V , A and T , as

$$\begin{aligned} S_I &= (1 + arm b_S)S_L - ar\tilde{c}_S S_{1\text{-link}} - \frac{arc'_S}{4}E_S \\ P_I &= (1 + arm b_P)P_L + ar\tilde{c}_P \partial_\mu A_{L,\mu} - \frac{arc'_P}{4}E_P \\ V_{I,\mu} &= (1 + arm b_V)V_{L,\mu} + arc_V \partial_\nu T_{L,\mu\nu} - ar\tilde{c}_V V_{1\text{-link},\mu} - \frac{arc'_V}{4}E_{V,\mu} \\ A_{I,\mu} &= (1 + arm b_A)A_{L,\mu} + arc_A \partial_\mu P_L - ar\tilde{c}_A A_{1\text{-link},\mu} - \frac{arc'_A}{4}E_{A,\mu} \\ T_{I,\mu\nu} &= (1 + arm b_T)T_{L,\mu\nu} + arc_T (\partial_\mu V_{L,\nu} - \partial_\nu V_{L,\mu}) - ar\tilde{c}_T T_{1\text{-link},\mu\nu} - \frac{arc'_T}{4}E_{T,\mu\nu}, \end{aligned} \quad (B4)$$

where, we have dropped all $O(a^2)$ terms, and for all \mathcal{O} , $b_{\mathcal{O}} = (2 - c_{swr})/2$, $c_{\mathcal{O}} = c_{swr}/4$ (except $c_T = -c_{swr}/4$), $c'_{\mathcal{O}} = 1 - c_{swr}$ and $\tilde{c}_{\mathcal{O}} = c_{swr}/4$. The local operators, \mathcal{O}_L , are defined as $\overline{\psi}\Gamma_{\mathcal{O}}\psi$ with $\Gamma_{\mathcal{O}}$ being 1, $\gamma_5 = \gamma_1\gamma_2\gamma_3\gamma_4$, γ_μ , $\gamma_\mu\gamma_5$ and $i\sigma_{\mu\nu} = -[\gamma_\mu, \gamma_\nu]/2$ for $\mathcal{O} = S, P, V_\mu, A_\mu$ and $T_{\mu\nu}$ respectively⁶; the equation of motion operators, $E_{\mathcal{O}}$, as $\overline{\psi}(\Gamma_{\mathcal{O}}\overrightarrow{\mathcal{W}} - \overleftarrow{\mathcal{W}}\Gamma_{\mathcal{O}})\psi$, and the 1-link operators $\mathcal{O}_{1\text{-link}}$ as

$$\begin{aligned} S_{1\text{-link}} &= \overline{\psi}\overleftrightarrow{\mathcal{D}}\psi \\ V_{1\text{-link},\mu} &= \overline{\psi}\overleftrightarrow{D}_\mu\psi \\ A_{1\text{-link},\mu} &= -i\overline{\psi}\overleftrightarrow{D}_\nu\sigma_{\nu\mu}\gamma_5\psi \\ T_{1\text{-link},\mu\nu} &= \epsilon_{\mu\nu\lambda\delta}\overline{\psi}\overleftrightarrow{D}_\lambda\gamma_\delta\gamma_5\psi, \end{aligned} \quad (B5)$$

where $\overleftrightarrow{D} = \overrightarrow{D} - \overleftarrow{D}$. It is easy to see that the operators \mathcal{O}_L , $\mathcal{O}_{1\text{-link}}$, and \mathcal{O}_{EM} form an over-complete basis for all dimension-4 fermion bilinear operators, and therefore no new operators

⁶ Ref. 8, a factor of i was inadvertently missed in the definition of $\sigma_{\mu\nu}$. The correct definition is $\sigma_{\mu\nu} = i[\gamma_\mu, \gamma_\nu]/2$.

are needed for non-perturbative improvement of the quenched theory. In this paper, we have chosen to eliminate the 1-link operators (and the $\partial_\mu A_\mu$ term in P_I) non-perturbatively by an appropriate choice of c_{swr} . At tree-level, this implies $c_{swr} = 0$, whereby

$$\begin{aligned} b_{\mathcal{O}} &= 1, \\ c_{\mathcal{O}} &= 0, \\ c'_{\mathcal{O}} &= 1. \end{aligned} \tag{B6}$$

It is important to note that beyond tree-level, the matrix elements of the 1-link operators have divergences proportional to a^{-1} , and hence contribute to the renormalization constants at $O(a^0)$. As a result, not only do the $O(a)$ correction terms $b_{\mathcal{O}}$, $c_{\mathcal{O}}$ and $c'_{\mathcal{O}}$ depend on the choice of $\tilde{c}_{\mathcal{O}}$, but so do $Z_{\mathcal{O}}^0$, except for $\mathcal{O} = P$.

APPENDIX C

In this appendix we give a brief description of the two exceptional configurations we found in the **60NP** data set. In both of these we find that the zero mode is localized over 5 – 10 timeslices. If the Wuppertal source overlaps with the zero mode then the norm of the pion propagator for quark mass κ_7 can be up to a factor of a hundred larger than the average over the remaining configurations. If, on the other hand, the source time slice does not overlap with the zero mode, then we observe a “normal” temporal fall-off in the pion correlator until it hits the zero mode, when it shows a large bump. These two anomalous behaviors are illustrated in Fig. 25.

[1] K. Symanzik, Nucl. Phys. **B226**, 187 (1983).
[2] K. Symanzik, Nucl. Phys. **B226**, 205 (1983).
[3] M. Lüscher, S. Sint, R. Sommer, and P. Weisz, Nucl. Phys. **B478**, 365 (1996), hep-lat/9605038.
[4] M. Lüscher, S. Sint, R. Sommer, P. Weisz, and U. Wolff, Nucl. Phys. **B491**, 323 (1997), hep-lat/9609035.
[5] M. Lüscher, S. Sint, R. Sommer, and H. Wittig, Nucl. Phys. **B491**, 344 (1997), hep-lat/9611015.
[6] M. Guagnelli and R. Sommer, Nucl. Phys. (Proc. Suppl.) **B63**, 886 (1998), hep-lat/9709088.
[7] M. Bochicchio, L. Maiani, G. Martinelli, G. C. Rossi, and M. Testa, Nucl. Phys. **B262**, 331 (1985).
[8] T. Bhattacharya, S. Chandrasekharan, R. Gupta, W. Lee, and S. Sharpe, Phys. Lett. **B461**, 79 (1999), hep-lat/9904011.
[9] G. Martinelli, G. Rossi, C. Sachrajda, S. Sharpe, M. Talevi, and M. Testa, Phys. Lett. **B411**, 141 (1997), hep-lat/9705018.
[10] C. Dawson, G. Martinelli, G. Rossi, C. Sachrajda, S. Sharpe, M. Talevi, and M. Testa, Nucl. Phys. (Proc. Suppl.) **63**, 877 (1998), hep-lat/9710027.
[11] G. M. de Divitiis and R. Petronzio, Phys. Lett. **B419**, 311 (1998), hep-lat/9710071.
[12] B. Sheikholeslami and R. Wohlert, Nucl. Phys. **B259**, 572 (1985).
[13] T. Bhattacharya, R. Gupta, W. Lee, and S. Sharpe, Nucl. Phys. (Proc. Suppl.) **83-84**, 902 (2000), hep-lat/9909092.

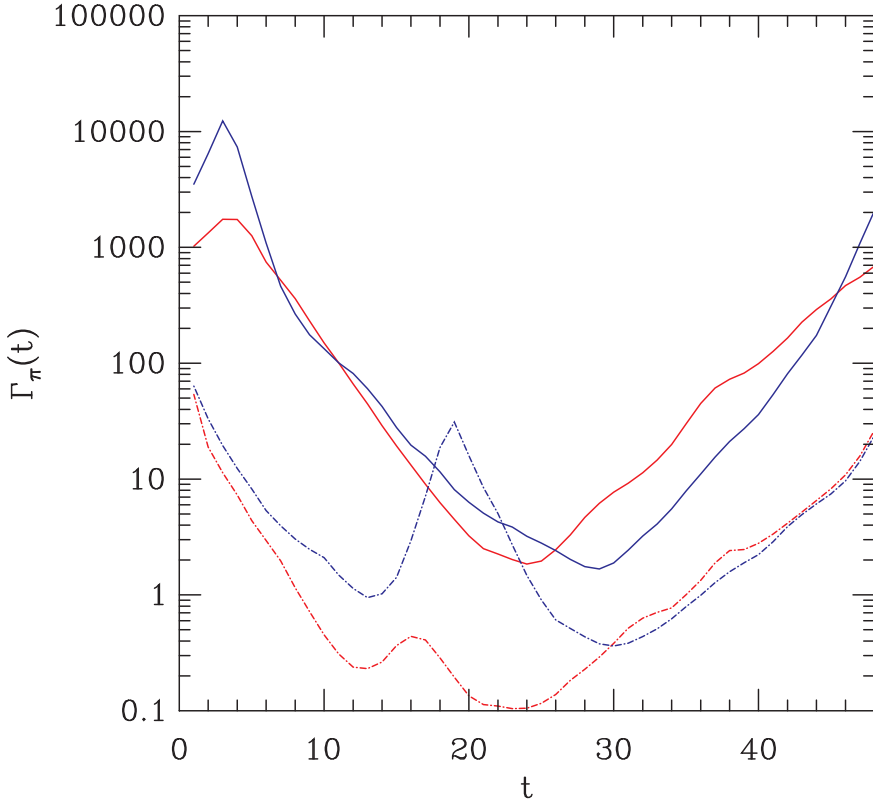


FIG. 25: Propagators on two exceptional configurations at $\beta = 6.0$. For each configuration we show the squared modulus of a quark propagator with $\kappa = \kappa_7$ and with the source (i) overlapping with the zero mode (solid line), and (ii) approximately 15 timeslices away from the zero mode (dashed line). Note the large amplitude if the source overlaps with the center of the zero mode, and the large deviation from exponential fall-off if it does not. In each case the time coordinates are translated so that the Wuppertal source is at $t = 1$.

- [14] M. Guagnelli, R. Sommer, and H. Wittig (ALPHA), Nucl. Phys. **B535**, 389 (1998), hep-lat/9806005.
- [15] R. Gupta, C. Baillie, R. Brickner, G. Kilcup, A. Patel, and S. Sharpe, Phys. Rev. **D44**, 3272 (1991).
- [16] R. Burkhalter *et al.* (CP-PACS), Nucl. Phys. (Proc. Suppl.) **73**, 3 (1999), hep-lat/9810043.
- [17] C. W. Bernard and M. F. L. Golterman, Phys. Rev. **D46**, 853 (1992), hep-lat/9204007.
- [18] S. R. Sharpe, Phys. Rev. **D46**, 3146 (1992), hep-lat/9205020.
- [19] G. Martinelli, C. Pittori, C. Sachrajda, M. Testa, and A. Vladikas, Nucl. Phys. **B445**, 81 (1995), hep-lat/9411010.
- [20] T. Bhattacharya, R. Gupta, G. Kilcup, and S. Sharpe, Phys. Rev. **D53**, 6486 (1996), hep-lat/9512021.
- [21] T. Bhattacharya, R. Gupta, and S. Sharpe, in preparation.
- [22] K. C. Bowler *et al.* (UKQCD), Phys. Lett. **B486**, 111 (2000), hep-lat/9911011.
- [23] M. Lüscher, private communication.
- [24] T. Bhattacharya, R. Gupta, W. Lee, and S. Sharpe, in preparation.
- [25] D. Becirevic, P. Boucaud, J. Leroy, V. Lubicz, G. Martinelli, F. Mescia, and F. Rapuano,

Phys. Rev. **D60**, 074501 (1999), hep-lat/9811003.

- [26] P. Lepage and P. Mackenzie, Phys. Rev. **D48**, 2250 (1993).
- [27] S. Sint and P. Weisz, Nucl. Phys. **B502**, 251 (1997), hep-lat/9704001.
- [28] S. Sint and P. Weisz, Nucl. Phys. (Proc. Suppl.) **63**, 153 (1998), hep-lat/9709125.
- [29] Y. Taniguchi and A. Ukawa, Phys. Rev. **D58**, 114503 (1998), hep-lat/9806015.
- [30] R. Wohlert, *Improved continuum limit lattice action for quarks*, unpublished; DESY 87/069.
- [31] M. Lüscher and P. Weisz, Nucl. Phys. **B479**, 429 (1996), hep-lat/9606016.
- [32] G. Heatlie, G. Martinelli, C. Pittori, G. C. Rossi, and C. T. Sachrajda, Nucl. Phys. **B352**, 266 (1991).